Heterogeneous photocatalysis and its potential applications in water and wastewater treatment: a review

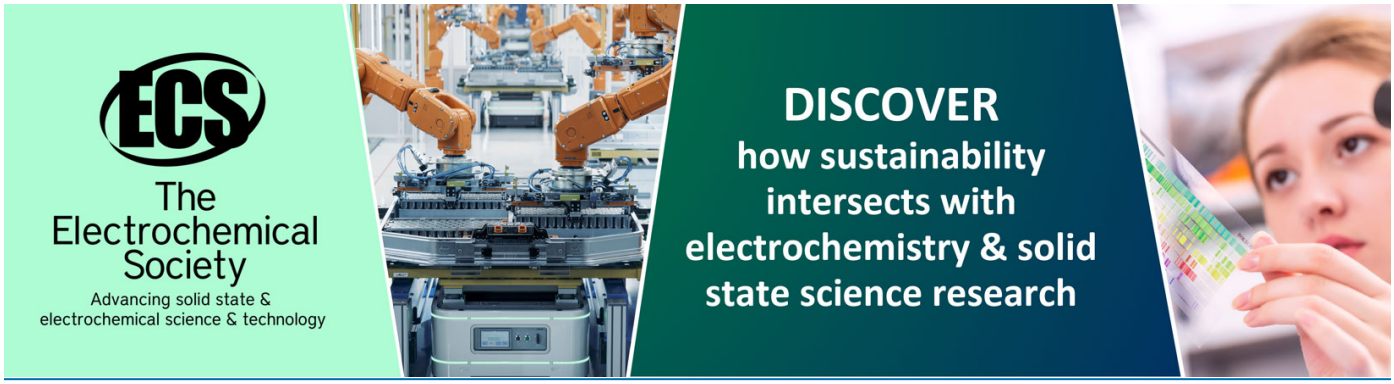

IOP Publishing Nanotechnology
Nanotechnology **29** (2018) 342001 (30pp) https://doi.org/10.1088/1361-6528/aac6ea

Topical Review

Heterogeneous photocatalysis and its potential applications in water and wastewater treatment: a review

Syed Nabeel Ahmed[1] and **Waseem Haider**[1,2]

[1] School of Engineering & Technology, Central Michigan University, Mt. Pleasant, MI 48859, United States of America
[2] Science of Advanced Materials, Central Michigan University, Mt. Pleasant, MI 48859, United States of America

E-mail: haide1w@cmich.edu

Received 7 March 2018, revised 3 May 2018
Accepted for publication 22 May 2018
Published 13 June 2018

Abstract

There has been a considerable amount of research in the development of sustainable water treatment techniques capable of improving the quality of water. Unavailability of drinkable water is a crucial issue especially in regions where conventional drinking water treatment systems fail to eradicate aquatic pathogens, toxic metal ions and industrial waste. The research and development in this area have given rise to a new class of processes called advanced oxidation processes, particularly in the form of heterogeneous photocatalysis, which converts photon energy into chemical energy. Advances in nanotechnology have improved the ability to develop and specifically tailor the properties of photocatalytic materials used in this area. This paper discusses many of those photocatalytic nanomaterials, both metal-based and metal-free, which have been studied for water and waste water purification and treatment in recent years. It also discusses the design and performance of the recently studied photocatalytic reactors, along with the recent advancements in the visible-light photocatalysis. Additionally, the effects of the fundamental parameters such as temperature, pH, catalyst-loading and reaction time have also been reviewed. Moreover, different techniques that can increase the photocatalytic efficiency as well as recyclability have been systematically presented, followed by a discussion on the photocatalytic treatment of actual wastewater samples and the future challenges associated with it.

Keywords: photocatalysis, heterojunction, nanomaterials, TiO_2, water treatment

(Some figures may appear in colour only in the online journal)

Nomenclature

AOPs	Advanced oxidation processes
BPA	Bisphenol A
CB	Conduction band
CDs	Carbon dots
E. coli	*Escherichia coli*
E_{bg}	Band gap
g-C_3N_4	Graphitic carbon nitride
GO	Graphene oxide
IM	Immobilized
LCA	Life cycle assessment
MB	Methylene blue

MC	Methylthionine chloride
MF	Microfiltration
MNPs	Magnetite nanoparticles
MO	Methyl orange
NF	Nanofiltration
NPs	Nanoparticles
PCOU	P-coumaric acid
PHA	Phthalic anhydride
PMR	Photocatalytic membrane reactors
rGO	Reduced graphene oxide
S. aureus	*Staphylococcus aureus*
TEM	Transmission electron microscopy
TNH	TiO_2 nanoholes structure
VB	Valence band
ZPC	Zero point charge

1. Introduction

Clean and drinkable water, free of toxic materials, carcinogenic substances and harmful bacteria, is necessary for human health. According to the United Nations' World Water Development Report 2018, the demand for clean water is expected to increase by nearly one-third by 2050 [1]. Clean water is a primary requirement in a variety of crucial industries including electronics, food and pharmaceuticals. Therefore, in order to meet the water supply demands, more and more efforts are being made to develop new methods for the reclamation of wastewater, both from industries and households. Innovations in nanoengineering and nanotechnology promise great improvements in water quality with the help of nanosorbents, bioactive nanoparticles [2], nanocatalysts and nanoparticle enhanced filtration [3]. At the nanoscale (1–100 nm), materials demonstrate significantly different physical and chemical properties from their bulk counterparts. Furthermore, a higher surface to volume ratio provides a dramatic increase in the surface reactivity. As a result, nanotechnology-based products that decrease the amount of toxic substances to sub-ppb levels can help to achieve water quality standards and reduce the health concerns.

In the past decade, visible-light photocatalytic activities of many nanomaterials such as nanoparticles and quantum dots of CdS [4, 5], $BiVO_4$ [6], nanoparticles and nanorods of ZnO [7, 8], and nanocubes of AgCl [9, 10] have been reported. The most widely studied of these nanomaterials, TiO_2, has been around for more than three decades now and shows excellent photocatalytic activity, anti-reflection, as well as self-cleaning ability [11]. In addition to this, TiO_2 also possesses hydrophilicity [11], long term stability [11] and high photo-reactivity, along with lower toxicity and costs than other semiconductors [11]. Furthermore, in order to provide magnetic separation to TiO_2, embedding an Fe_3O_4 core has been proven very useful [12]. Fe_3O_4, being a photocatalyst itself, possesses superparamagnetic behavior at particle sizes below 20 nm, due to the finite size effect [13, 14]. This property, along with its photocatalytic ability, has been reported to be promising for water and wastewater treatment technology by many researchers [15–18]. Similary, ZnO, a wide band-gap semiconductor, and g-C_3N_4, a metal-free photocatalyst have recently emerged as promising materials for photocatalytic applications [19–22].

Another very important member of the photocatalytic family is graphene, which is formed by a two-dimensional array of hexagonal sp^2 hybridized carbon atoms. Since its discovery in 2004 [23], graphene and it derivatives have gained significant attention in many applications, with photocatalytic nanocomposites being one of them. Graphene has a unique two-dimensional structure, with high surface area, high conductivity and electron mobility. Consequently, graphene can potentially promote electron–hole recombination more effectively and thus improve the photocatalytic efficiency [24].

These semiconductors have the potential to degrade the contaminants and microorganisms from the water and waste water, through a process called heterogeneous photocatalysis. Heterogeneous photocatalysis utilizes photon energy and converts it into chemical energy, and offers great potential for many applications specially water and waste water treatment. This process is really effective in degrading a wide range of organic contaminants, eventually mineralizing them into carbon dioxide and water [25]. Therefore, unlike other water treatment techniques such as coagulation and flocculation, heterogeneous photocatalysis completely eliminates the contaminants, rather than transforming them from one phase to another.

2. Heterogeneous photocatalysis

A fast-growing population and ever-improving industrialization has rendered the problem of wastewater very vital in the recent years, and consequently lead to researchers studying the advanced oxidation processes (AOPs), and looking for solutions. Among the AOPs, semiconductor photocatalysis has emerged as a promising technique which has the potential for total mineralization of the organic pollutants [26–29] as well as toxic metal ions [30, 31]. Since the discovery of the photocatalytic properties of TiO_2 in 1972 [32], there has been lots of research devoted to the understanding of fundamental mechanisms and parameters in order to utilize this process for water and wastewater treatment applications.

The mechanism of heterogeneous photocatalysis is primarily described by the semiconductors' capability to generate charge carriers under light irradiation followed by the generation of free radicals such as OH- which leads to further reactions, eventually forming CO_2 and H_2O [33]. Therefore, the most attractive features of heterogeneous photocatalysis include [34]:

- The pollutants degrade into CO_2 and other inorganic substances completely.
- The process takes place at ambient conditions.

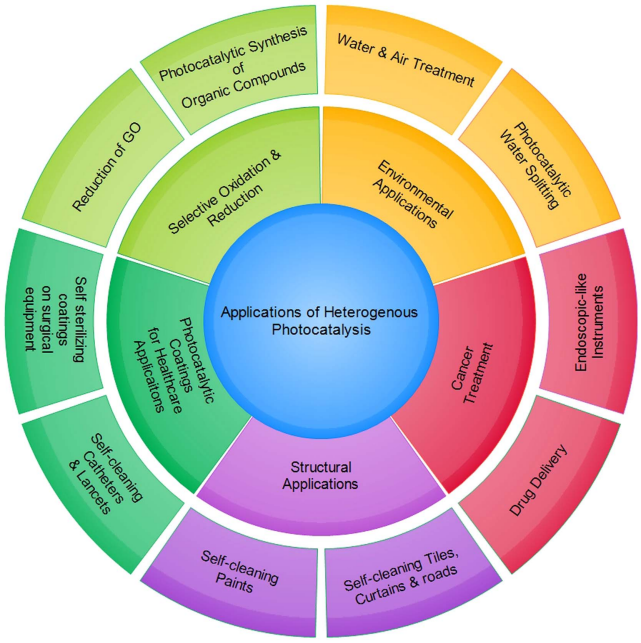

Figure 1. Potential applications of heterogeneous photocatalysis.

- The only requirement for the reaction to initiate is the presence of oxygen and ultra-bandgap energy, both of which can directly be obtained from the air and sun.
- It is possible to support the catalyst on various types of inert matrices which include glasses, polymers, carbon nanotubes and graphene oxides [35–37].
- The catalyst is cheap, non-toxic and reusable.

Figure 1 demonstrates the potential applications of heterogeneous photocatalysis in environmental, medical and structural applications. The self-sterilizing character of TiO_2 along with its photocatalytic property can be used in the manufacturing of self-cleaning paints, tiles, surgical equipment, roads, and in the preservation of food [38, 39]. Moreover, heterogeneous photocatalysis is one of the cheapest and eco-friendly methods for water as well as air purification [40, 41].

2.1. Mechanism of heterogeneous photocatalysis

The mechanism of heterogeneous photocatalysis involves a chain of oxidative and reductive reactions on the surface of the photocatalyst. In a semiconductor, the lowest occupied and the highest unoccupied energy bands are divided by a bandgap, denoted by E_{bg}. When light energy (photons) carrying a photon energy greater than or equal to E_{bg} of the semiconductor is illuminated on its surface, the electrons from the valence bands are photo-excited and promoted to conduction band (CB) in femtoseconds. This leaves behind an unfilled valence band, called a hole (h^+), thus creating an electron–hole pair. If these electrons and holes are somehow trapped on the semiconductor surface and their recombination is prevented, this initiates a series of reactions postulated as follows [42]:

$$\text{Photoexcitation: } TiO_2 + h\nu \rightarrow e^- + h^+, \quad (1)$$

$$\text{Entrapment of free electrons: } e^-_{CB} \rightarrow e^-_{TR}, \quad (2)$$

$$\text{Entrapment of holes: } h^+_{VB} \rightarrow h^+_{TR}, \quad (3)$$

$$\text{Charge carrier recombination: } e^-_{TR} + h^+_{VB} \rightarrow e^-_{CB} + \text{heat}, \quad (4)$$

$$\text{Photoexcited electron scavenging: } (O_2)_{ads} + e^- \rightarrow O_2^-, \quad (5)$$

$$\text{Oxidation of hydroxyls: } OH^- + h^+ \rightarrow OH\cdot, \quad (6)$$

$$\text{Photodegradation by } OH^- \text{ radicals: } R - H + OH\cdot \rightarrow R'\cdot + H_2O. \quad (7)$$

The $OH\cdot$ radicals generated in equation (6) reduces organic impurities into intermediate compounds, which are further degraded by the same reaction until CO_2 and water are released as by-products (equation (7)). The overall reaction can be summarized into the following steps [42]:

i. Mass transfer of the organic pollutants or bacteria from the bulk liquid phase to the photocatalyst surface.
ii. Adsorption of the pollutant into the photon activated photocatalyst surface.
iii. The generation of $OH\cdot$ radicals and H_2O_2 followed by the chemical degradation of the contaminants.
iv. Desorption of the intermediate or final products from the surface of the photocatalyst.
v. Mass transfer of the intermediate or final product into the bulk liquid phase [42].

2.2. Applications

2.2.1. Water and waste water treatment. One of the main applications of semiconductor photocatalysis comes in water and waste water purification. In photocatalysis, the main role of these semiconductors is to transfer the energy from the light to the charge carrier [43]. TiO_2 and ZnO are wide bandgap semiconductors with strong adsorption in the UV, making them ideal for efficiently photodegrade many organic impurities and toxic metal ions as discussed previously. Recently, this process has also been found useful on actual water samples from Agbo river [29]. Moreover, these semiconductors can also be used for the treatment of seawater in case of oil spills, particularly for the removal of water-soluble fractions of crude oil [44–47].

2.2.2. Air treatment. Air pollutants, specially sulfur dioxide and nitrates, have the potential to generate persistent negative impacts on the human health. Just like water purification, TiO_2 is the most widely studied photocatalyst for air purification as well. TiO_2, in the form of coatings and nanotubes, have been successfully tested on the removal of acetone [48], ethanol [48], toluene [40, 48], and volatile organic compound [49]. In the past few years, graphitic

carbon nitride (g-C_3N_4) has also demonstrated great potential for air purification even with visible light irradiation [41, 50].

2.2.3. Reduction of GO. The reduction of GO to rGO has been done in many different ways in the past decade to increase its electronic conductivity. Recently, photocatalytic-induced reduction mechanisms have been demonstrated as effective methods for the reduction of GO. Such methods have also been used for the preparation of rGO–TiO_2 [51] and rGO–ZnO nanocomposites [52]. This has been achieved by hybridizing graphene oxide with both TiO_2 as well as ZnO [52, 53]. The photocatalytic technique provides an on-demand UV-assisted reduction technique for graphene oxide by producing photogenerated electrons on the semiconductor under UV-light irradiation. These photogenerated electrons are subsequently transferred to the GO nanosheets, resulting in the formation of rGO [54].

2.2.4. Selective oxidation and reduction of organics. Although photocatalysis has been considered an unselective process for a long period of time specially in water, the field of selective photocatalysis has developed rapidly in recent years. This newly developed field has now extended to several applications such as the production of aromatic aldehydes [55], oxidation of alcohols [56, 57] and the photocatalytic reduction of CO_2 for energy applications [58–60]. Selective oxidation and reduction can be achieved by modifications of the photocatalyst or by the alterations in the external conditions [61].

2.2.5. Targeted drug delivery. Surface engineered iron oxide nanoparticles can effectively be employed in drug delivery applications. As magnetic vectors can be directed to the target of interest using magnetic field, these magnetic nanoparticles have been designed to deliver DNA molecules, peptides, and radioactive chemotherapeutic, and hyperthermic drugs for localized damage of tumor tissue [62]. The attachment of radiotracers to Iron oxide nanoparticles can also aid in radio-labeled magnetic drug delivery systems, allowing a higher local dose to enhance tumor cell eradication [62].

3. Application of heterogeneous photocatalysis for water and wastewater treatment

3.1. Photocatalytic materials

Some of the most widely used photocatalytic nanomaterials include Fe_3O_4, TiO_2, ZnO, and graphitic carbon nitride (g-C_3N_4). The features and properties of these nanomaterials specially magnetite (Fe_3O_4) nanoparticles (MNPs), ZnO and TiO_2 for heterogeneous photocatalysis have been briefly discussed in the previous literatures [30, 31, 63–65], and will be discussed in this paper too. These nanomaterials and their combinations carry an enormous potential for water and wastewater treatment and will be discussed later in this paper.

Besides the fore-mentioned nanomaterials, another very important member of the photocatalysis family is graphene oxide, which is also one of the most emerging advanced nanomaterial of the 21st century. Out of its countless number of applications, heterogeneous photocatalysis is one of the most phenomenal. The ballistic behavior of graphene has been in discussion for the past 20 years [66]. Combination of this character with graphene oxide being hydrophilic in nature, provides higher efficiency of the water purification processes [30, 67].

In a broader way, photocatalytic nanomaterials can be categorized in terms of dimensionality as zero-dimensional (nanoparticles [68] and quantum dots [69]), one-dimensional (nanorods [70, 71], nanoribbons [72], and nanotubes [4, 72]), two-dimensional (graphene bases nanocomposites) [66, 73, 74], or three-dimensional (3D graphene) [21, 75, 76]. The choice of morphology depends upon the targeted application, as well as the desired properties. The most widely used group of nanomaterials is the zero-dimensional group, particularly in the form of core–shell nanoparticles.

3.1.1. Core–shell nanoparticles. Since the discovery of sandwich colloidal semiconductor particles in the 1980s [77], the creation of multilayered nanoparticles has become a significant research area in advanced materials chemistry today [78]. In the 1990s, the researchers developed concentric multilayer semiconductor nanoparticles and the term 'core–shell' was adopted. The core–shell particles, as the name implies consist of an inner material (core) and an outer material (shell). Figure 2 shows different forms of core–shell particles used in many technological areas such as quantum dots, microelectronics, optic, magnetic, and photoactive devices [77, 78]. However, the primary focus of this article constitutes of the photocatalytic applications.

Among all these core–shell structures, Fe_3O_4 based core–shell structures have been exclusively studied, due to the fact that an Fe_3O_4 core aids with the magnetic separation of the nanocomposite from the aqueous medium. Singh *et al* and Wu prepared Fe_3O_4 embedded ZnO nanocomposite and compared its magnetic properties with pure Fe_3O_4. The curves (a) and (b) in figure 3(b) show the M versus H loop of pure Fe_3O_4 and Fe_3O_4 @ ZnO respectively [79]. It has been observed that Fe_3O_4 nanoparticles embedded in ZnO provide much higher photocatalytic efficiency as compared to their individual counterparts, as compared in figure 3(a) [31]. Moreover, the resulting nanocomposite demonstrates almost the same photocatalytic efficiency in the second and third cycle of use. Thus core–shell structure provides an effective way to combine the beneficial properties of two or more nanomaterials into one nanocomposite.

3.1.2. Nanocomposites and heterojunctions. Heterojunction is defined as the interface between two different semiconductors with unequal band structure. Typically, there are three types of conventional semiconductor heterojunctions; namely (i) straddling type (ii) staggered type, and (iii) those with a broken gap. In type-I (straddling type heterojunctions), the energy band gap of semiconductor A is wider than B, (as

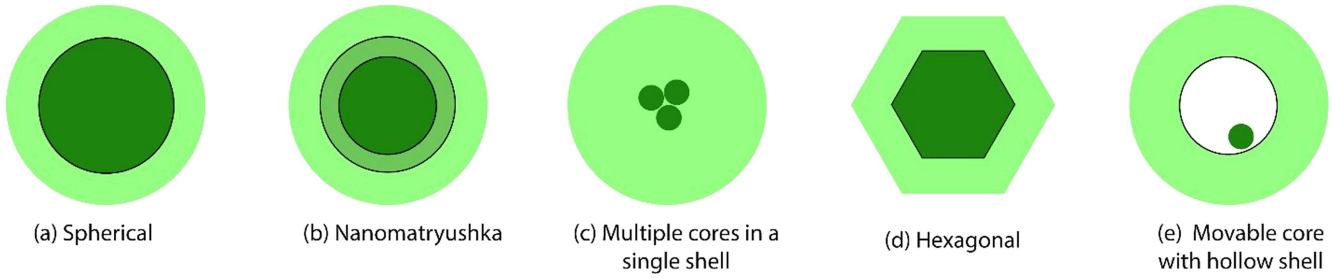

Figure 2. Various forms of core/shell nanoparticles. (Reprinted (adapted) with permission from Chaudhuri and Paria [77]. Copyright 2011 American Chemical Society.)

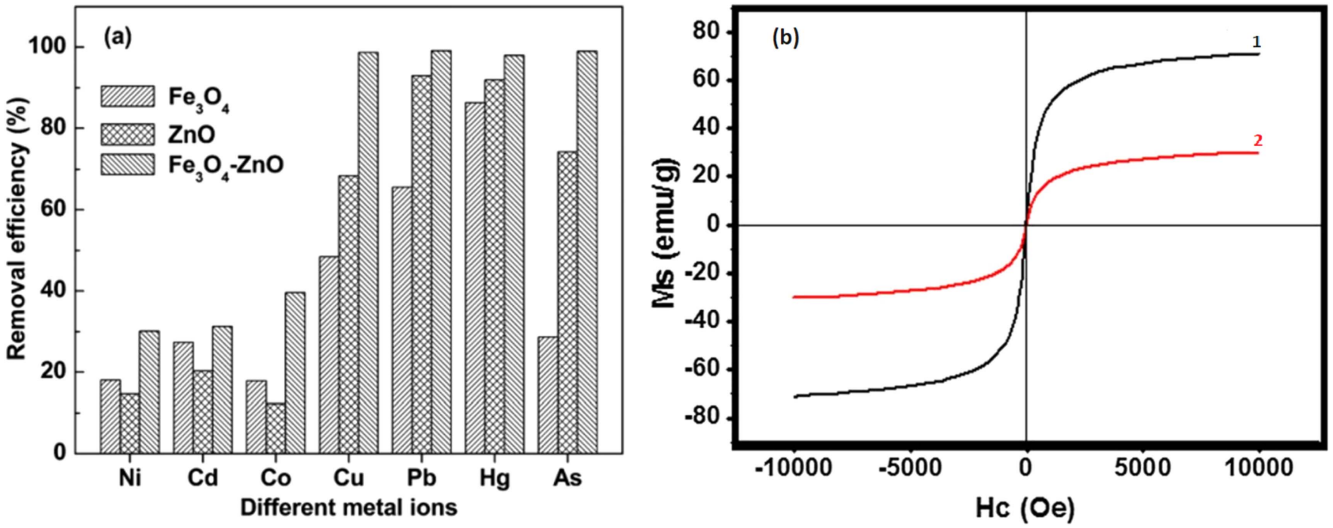

Figure 3. (a) Comparison of removal efficiencies of toxic metal ions by Fe_3O_4, ZnO and Fe_3O_4–ZnO. Reproduced from [31] with permission from The Royal Society of Chemistry. (b) Magnetic hysteresis loop (M versus H) of (a) pure Fe_3O_4 and (b) Fe_3O_4 @ ZnO(right). Reprinted by permission from Springer Nature Journal of Materials Science: Materials in Electronics [79] Copyright 2016.

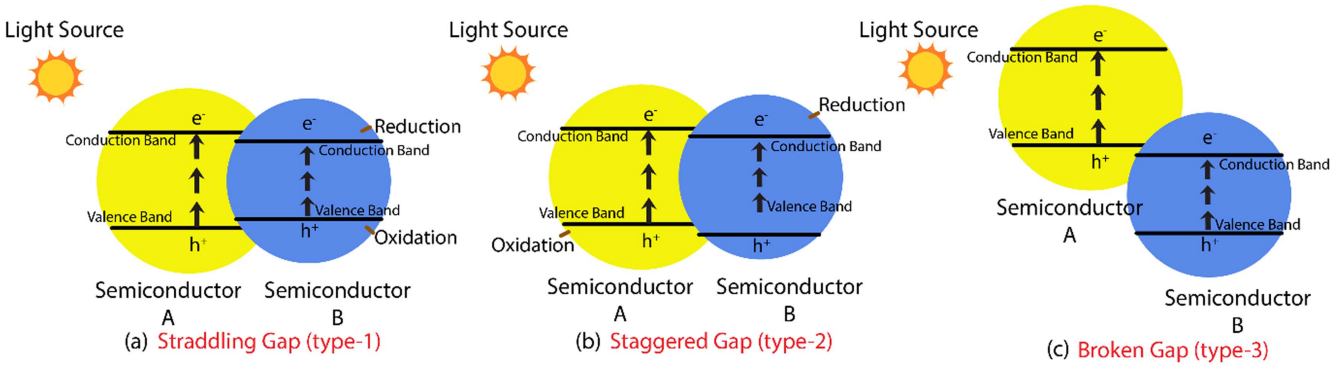

Figure 4. Types of conventional heterojunction (a) straddling gap, (b) staggered gap, (c) broken Gap.

shown in figure 4), resulting in the accumulation of the charge carriers on the semiconductor with smaller band gap. Since both electron and hole are accumulated on the same semiconductor, the recombination of charge carriers is still possible. In type-II (staggered type) heterojunction, the valence and CBs of semiconductor A are higher and lower than those of B. This results in the spatial separation of charge carriers which prevents the recombination of electrons and holes. The type-III heterojunction (with broken gap) is the same as the staggered type except that the staggered gap becomes so wide that electron–hole migration is not possible, therefore, the separation cannot occur [35, 77].

Besides conventional heterojunction, many other forms of heterojunctions have also been studied. These include p–n heterojunction, surface heterojunction, direct Z-scheme heterojunction and semiconductor/graphene heterojunction. A p–n junction improves the photocatalytic performance by providing an additional electric field. This is achieved by combining n-type and p-type semiconductors. On the other hand, a surface heterojunction involves creating different

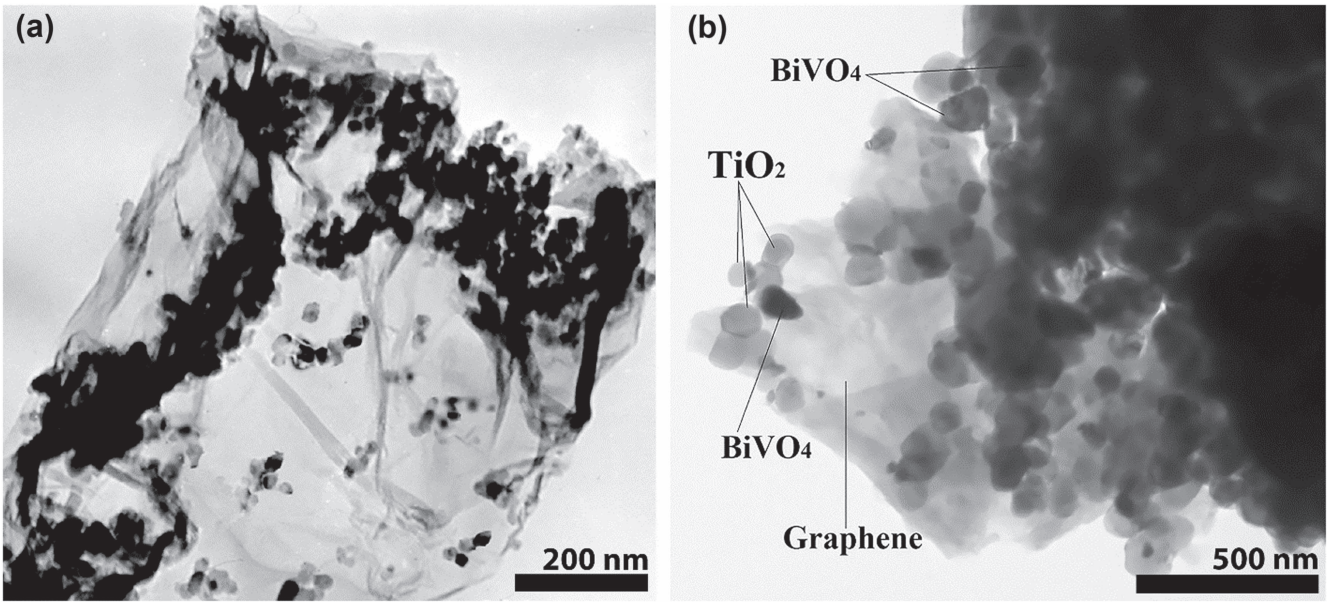

Figure 5. (a) TEM image of TiO_2-graphene nanocomposite prepared by Zhang (Reprinted by permission from Springer Nature Journal of Materials Science (full set) [92]. Copyright 2017) (b) TEM image of a ternary $GO/BiVO_4/TiO_2$ nanocomposite. Reprinted (adapted) with permission from Zhang *et al* [90], Copyright 2010 American Chemical Society.

crystal facets on the exposed surface of a semiconductor [35, 80, 81]. Although these heterojunctions tend to enhance the electron–hole separation, they also reduce the redox ability of the photocatalyst. In order to overcome this problem, Z-scheme heterojunction has been employed to maximize the redox potential of the heterojunction systems. Z-scheme photocatalytic system consists of two different semiconductors, and an acceptor/donor pair. The two semiconductors are not in a physical contact, instead the migration of the photogenerated holes takes place through the acceptor/donor pair [35, 77, 82, 83].

Recently, a new form of heterojunction, called semiconductor/graphene heterojunction has gained huge interest [35, 73, 77, 84–89]. Due to the ultrahigh electron conductivity of graphene, the electron flow is enhanced, consequently improving the photocatalytic efficiency. Moreover, a large π–π conjugation on the graphene surface can be useful in the adsorption of different reactants during the photocatalytic reaction. However, it has been observed that if the graphene content is higher than 1% by weight, the photocatalytic activity of the semiconductor is drastically affected, due to the light shielding effect which suppresses the semiconductor irradiation [35]. In the past few years, many semiconductor graphene heterojunctions such as TiO_2-graphene, ZnO-graphene, CdS-graphene and C_3N_4-graphene have been studied [5, 83, 90, 91].

Figure 5 illustrates a typical TEM micrograph of a TiO_2-graphene nanocomposite, as prepared by Zhang *et al* by using facile one step hydrothermal method [92]. Zhang and coworkers reported efficient charge separation properties, excellent absorptivity of dyes, and extended light absorption range simultaneously. Similarly, figure 5(b) shows the TEM image of a ternary nanocomposite of $RGO/BiVO_4/TiO_2$ [90]. These nanocomposites have been prepared by hydrothermal methods and can be used in many environmental applications including, but not limited to, water and wastewater treatment [93].

3.2. Potential nanomaterials for water and wastewater purification

3.2.1. Ferritic nanomaterials. Ferritic nanomaterials include magnetite (Fe_3O_4) NPs, maghemite (γ-Fe_2O_3) NPs and nanorods, and hexagonal ferrites. One of the key features of Fe_3O_4 catalyst is its easy recovery by magnetic force and its reusability due to its long term stability [26]. Magnetic nanoparticles display the finite size effect of high surface to volume ratio, resulting in an excellent adsorption capacity for the removal of toxic metal ions [63, 94].

Fe_3O_4, being the most widely studied photocatalyst among the ferrite nanoparticles, displays exceptional superparamagnetic behavior, which provides an additional benefit of a much easier magnetic separation of the semiconductor and the solution. The preparation of Fe_3O_4 nanoparticles is commonly done by coprecipitation method [13, 31, 63, 79] or thermal decomposition method [95–98], with slight variations such as the room temperature coprecipitation by Mascolo and sonochemical preparation by Solomon [13, 26, 99]. Moreover, different variations in the morphologies of ferritic nanoparticles are shown in figures 6(a) and (b), which show the SEM images of hollow Fe_2O_3 nanoparticles [100] and a complex core–shell nanocomposite of Fe_3O_4 @ SiO_2 @ Poly (ethyleneimine)-Au/Ag @ Polydopamine [101]. These nanocomposites show highly stabilized reactivity and magnetic recyclability. Table 1 summarizes different studies of the photocatalytic activities of Fe_3O_4.

3.2.2. ZnO. Zinc oxide is a wide-bandgap semiconductor with a large exciton binding energy of 60 meV and a bandgap

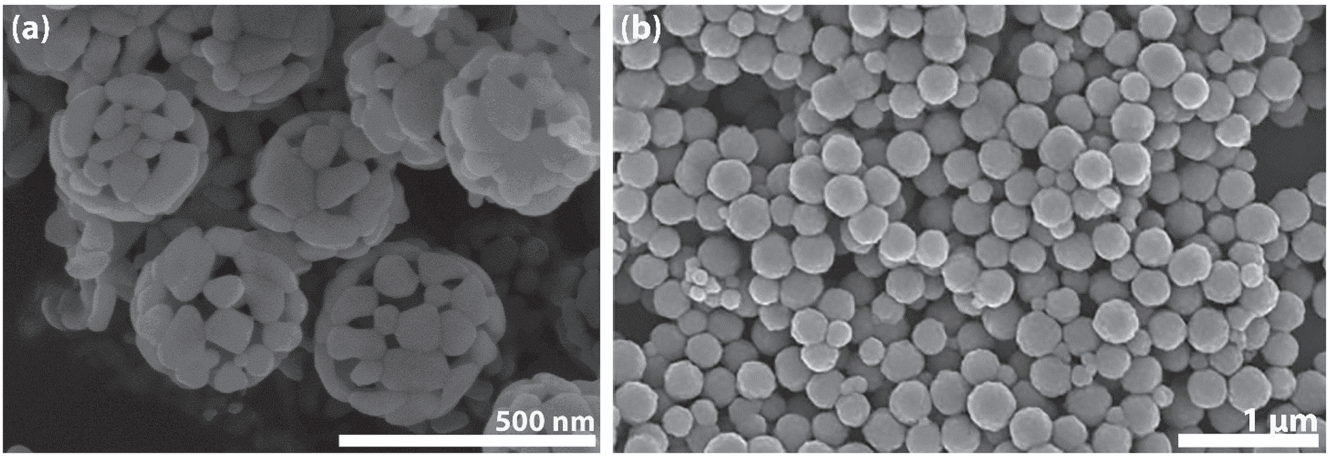

Figure 6. (a) SEM image of hollow Fe_2O_3 nanoparticles (Reprinted (adapted) with permission from Yu *et al* [100]. Copyright 2009 American Chemical Society.) and (b) SEM image of a complex Fe_3O_4@SiO_2@Poly(ethyleneimine)-Au/Ag@Polydopamine nanocomposite (Reprinted from Yu *et al* [101]. Licensed under Creative Commons Attribution 4.0 International License (http://creativecommons.org/licenses/by/4.0/). © 2016 Springer Nature.).

of 3.37 eV. These two properties make it suitable for a variety of environmental, optical and electronic applications [68, 107]. Semiconductor ZnO nanoparticles display excellent photocatalytic efficiency against the organic contaminants due to their non-toxic nature, wide band gap, and good quantum efficiency [31]. Furthermore, the past decade has witnessed a rising interest in the photocatalytic applications of ZnO due to the fact that researchers have reported ZnO showing more impressive photocatalytic properties than widely studied TiO_2 [68]. The electron mobility of ZnO ($\sim$100 $cm^2 V^{-1} s$) is approximately two orders of magnitude higher than TiO_2 based nanomaterials. Thus, it is easier for the photo-generated charge carriers to migrate towards the surface of ZnO-based nanomaterials [108]. The excellent photocatalytic efficiency of ZnO also comes from the creation of defect sites which prevents the electron–hole recombination by photon absorption. ZnO can be synthesized in many different morphologies, as reported by Xu *et al* some of which are shown in figure 7. These include cauliflower-like, truncated hexagonal, nanotubes, and hourglass-like morphologies [109]. Additionally, ordered ZnO nanowall arrays and single-crystal ZnO are much easier to be synthesized with high aspect ratios, because of its tendency for natural anisotropic growth [20, 108, 110]. ZnO has also been proven to be useful in the removal of toxic metal ions as well as harmful microorganisms such as *Escheria coli* (*E.coli*) and *Staphylococcus aureus* (*S. aureus*) [31]. Table 2 summarizes the recent advances in ZnO-based nanocomposites and their photocatalytic performances.

3.2.3. TiO_2. TiO_2 in anatase crystalline form is the most widely studied photocatalyst because of its high quantum yield which is mainly responsible for its photocatalytic efficiency [27, 116]. The bandgap energy of 3.2 eV for TiO_2 requires photoexcitation wavelengths less than 385 nm, corresponding to a near-UV light irradiation. TiO_2 is considered the most efficient photocatalyst in the removal of bacteria and organic contaminants [117–121]. The behavior of TiO_2 in attracting all the micro level impurities such as metal ions (e.g. Pb^{+2} and Cr^{+6}) and dissolved minerals has also been extensively studied [7, 31, 33, 105, 111, 122], along with its self-sterilizing property. The results have shown that when doped with nitrogen ions or metal oxides, the photocatalytic behavior of TiO_2 can be achieved in visible light too [43]. Additionally, TiO_2 particles, being extremely versatile, can act as both oxidative and reductive catalysts for the removal of organic and inorganic impurities [123]. Due to its self-sterilizing property, it can be used in many biomedical applications such as on-demand bactericidal properties in dental adhesives [124], catheters and other medical tubes [39].

3.2.3.1. Visible light responsive TiO_2. Several studies have shown that, with various kinds of doping and heterojunctions, the TiO_2 photocatalysis can be achieved in the visible light as well [82, 119, 125]. One of the methods to achieve this is by coupling TiO_2 with a narrow bandgap semiconductor. Zhu and Guo used the same approach by coupling TiO_2 with CdS, which has a bandgap of 2.4 ev [4, 126]. When TiO_2 is coupled with CdS, it has been reported that the formation of heterojunction at the contact interface can hinder the charge carrier recombination controlling the charge separation. Additionally, due to the synergistic effect, both TiO_2 and CdS are irradiated and activated simultaneously under incident light [4]. Recently, Zada fabricated a novel Ag–TiO_2 photocatalyst by using cicada wings as a template. This nano-holes/nano-nipples structure has demonstrated remarkable photocatalytic activity in UV–visible light by completely degrading MB dye in 15 min This excellent photocatalytic activity is attributed to the high surface area, enhanced electron–hole separation, and localized surface plasmon resonance property of Ag NPs. Figures 8(a) and (b) illustrate the TEM images of this nano-holes/nano-nipple structure [127].

Apart from heterojunction, TiO_2 photocatalysis can also be achieved in visible light by doping in with nitrogen or sulfur [128–131], or co-doping with both [132]. Copper

Table 1. Photocatalytic performance of Fe_3O_4 with various heterojunctions.

Composition	Light source	Pollutant	Experimental conditions	Dimensionality	PE	References
Fe_3O_4	UV	Methyl red	CL = 0.075 g l^{-1} t_r = 60 min	0D	50.5%	[26]
Fe_3O_4@ZnO	250 W UV	Rhodamine B (7 mg l^{-1})	CL = 1 g l^{-1} t_r = 60 min	0D	99.3%	[102]
Fe_3O_4–ZnO-$CoWO_4$	50 W visible	Rhodamine B (4.8 mg l^{-1})	CL = 0.4 mg l^{-1} t_r = 405 min	0D	98.3%	[103]
Fe_3O_4@TiO_2	250 W UV	Rhodamine B (10 mg l^{-1})	CL = 0.2 g l^{-1} t_r = 60 min	0D	92%	[17]
Bi_2O_3–Fe_3O_4	15 × 6 W visible	Ibuprofen (2.1 mg l^{-1})	CL = 0.2 g l^{-1} t_r = 120 min	1D	~100%	[104]
Fe_3O_4–CuO–ZnO-Nano graphene	40 W UV	Methylene blue (30 mg l^{-1})	CL = 0.3 g l^{-1} t_r = 120 min	2D	93%	[64]
Fe_3O_4@Bi_2O_3-30%rGO	Visible	Ciprofloxacin	CL = N/A t_r = 240 min	2D	98.3%	[105]
Fe_3O_4–ZnO–rGO	Visible	Methylene violet (408 mg l^{-1})	CL = 40 mg l^{-1} t_r = 120 min	2D	83.5%	[106]

Note. PE = photodegradation efficiency.
CL = catalyst loading.
t_r = irradiation time.

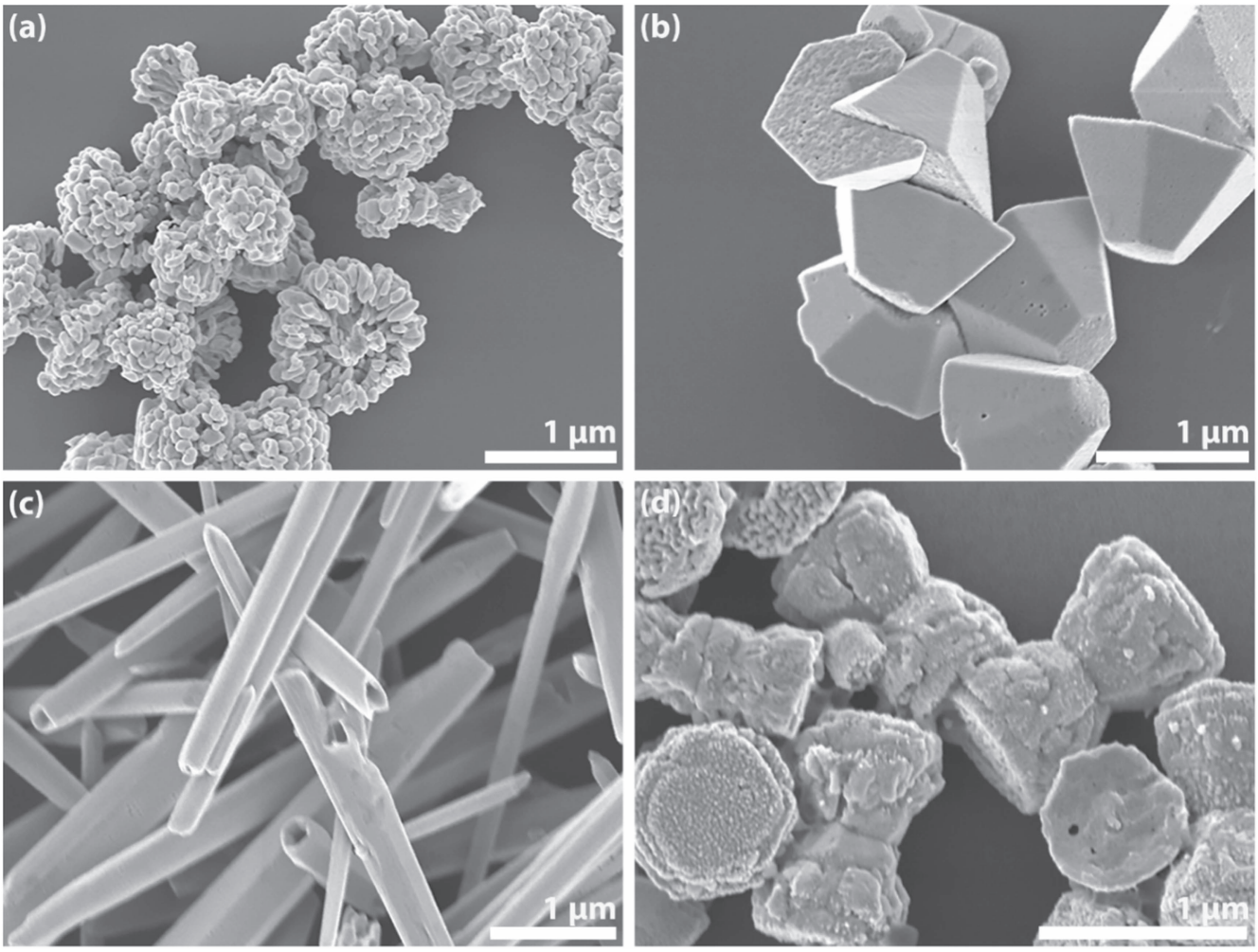

Figure 7. FESEM images of various ZnO morphologies showing (a) cauliflower-like, (b) truncated hexagonal, (c) nanotubes and (d) hourglass-like morphologies (Reprinted (adapted) with permission from Xu *et al* [109]. Copyright 2009 American Chemical Society.).

doped TO_2 films have also been found to accelerate the TiO_2 disinfection in the presence of natural sunlight [131]. Table 3 summarizes various nanocomposites of TiO_2 and their photocatalytic performance in UV and visible regions.

3.2.4. Carbon-based nanomaterials. Carbon-based nanomaterials include graphene, graphene oxide, reduced graphene oxide, fullerene, single and multi-walled carbon nanotubes [74]. Graphene, since its discovery in 2004 [23], has particularly received the most attention among the carbon-based nanomaterials. Graphene is essentially a two-dimensional structure formed by the hexagonal rings of sp^2 hybridized carbon atoms, and is considered the precursor for graphene family nanomaterials. It has a large theoretical specific surface area ($2630\ m^2\ g^{-1}$), high thermal conductivity ($\sim 5000\ W\ mK^{-1}$) high Young's modulus (~ 1.0 TPa) and good electrical conductivity [136]. Its excellent electron conductivity permits the flow of electrons from the semiconductor to its surface, preventing the electron–hole recombination. Additionally, the potential of graphene/graphene– (-0.08 V versus standard hydrogen electrode, pH = 0) is usually lower than the conduction-band potential of the semiconductor, thereby enabling the rapid electron migration from the semiconductor to the graphene. Furthermore, the large specific surface area of graphene helps to provide more active sites for the photocatalytic reactions to take place [35].

It has been proved by many studies that graphene-TiO_2 heterojunction provides much higher photocatalytic efficiency than pure TiO_2 [85, 86, 137–139]. Table 4 shows the effect of graphene hybridization on the photocatalytic performance of TiO_2 for the degradation of different contaminants.

The recently developed three-dimensional graphene (3DG) has also attracted increasing attention owing to its unique features. 3DG, with foam-like macrostructures, possesses many desirable properties, which include increased surface area, controlled shape and size, and ease of handling and reuse. These features make it a promising candidate for photocatalytic applications [21, 86]. Another pioneer in this category are carbon dots which have also emerged as a promising metal-free photocatalyst for photocatalytic applications, due to their excellent electron transfer rates, tunable optical absorption and emission, and good adsorption of organic molecules [69, 145]. The nanocomposites of ZnO with 3D graphene oxide have particularly gained more

Table 2. Photocatalytic performance of ZnO-based nanocomposites.

Composition	Light source	Pollutant	Experimental conditions	Dimensionality	PE	References
Pd(1%)–ZnO	UV (355 nm)	S. aureus (4×107 CFU ml^{-1})	CL = 1 g l^{-1} t_r = 10 min	0D	~100%	[111]
ZnO–CeO_2	250 W visible	Methylene blue	CL = 1 g l^{-1} t_r = 2.5 h	1D	97.4%	[8]
Ag–ZnO	1500 W UV	Phenol (20 mg l^{-1})	CL = 1 g l^{-1} t_r = 60 min	1D	58%	[22]
ZnO@Ag@ Cu_2O	12 W UV	Methyl orange (20 mg l^{-1})	CL = IM t_r = 240 min	1D	~64%	[112]
ZnO-graphene	UV (365 nm)	Deoxynivalenol (15 mg l^{-1})	CL = 0.5 mg l^{-1} t_r = 30 min	2D	~99%	[84]
Ag-ZMNWA[a]	50 W visible	MC (0.5 mg l^{-1})	CL = IM t_r = 90 min	2D	93.4%	[20]
CdS–ZnO-graphene	300 W visible	4-nitroaniline (10 mg l^{-1})	CL = 0.25 g l^{-1} t_r = 16 min	2D	98%	[113]
ZnO–GO	250 W UV	Methylene blue (960 mg l^{-1})	CL = 0.25 g l^{-1} t_r = 450 min	2D	~75%	[114]
Au–ZnO–rGO	UV and visible	Rhodamine B	CL = IM t_r = 180 min	3D	94%	[21]
Au–GO–ZnO	20 W UV	Methylene blue (3.2 mg l^{-1})	CL = IM t_r = 240 min	3D	81%	[115]
ZnO–rGO	20 W UV	Methylene blue (25 mg l^{-1})	CL = 0.1 g l^{-1} t_r = 60 min	3D	~86%	[76]

Note. PE = photodegradation efficiency.
MC = methylthionine chloride.
IM = immobilized.
t_r = irradiation time.
CL = catalyst loading.
[a] Ag–ZnO mesoporous nanowall arrays.

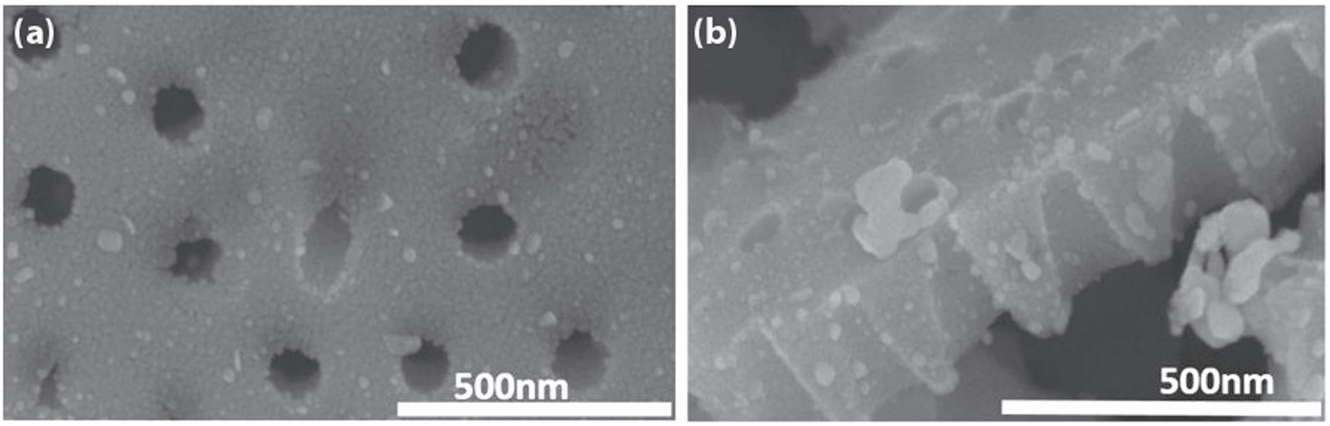

Figure 8. SEM images of the biomorphic Ag–TiO_2 photocatalyst showing (a) nano-holes on one side, and (b) nano-nipples on the other side (Reprinted from Zada *et al* [127]. Licensed under Creative Commons Attribution 4.0 International License (http://creativecommons.org/licenses/by/4.0/). © 2017 Springer Nature.).

attention due to the increased surface area enhanced photocatalytic activity resulting from effective charge transfer from ZnO to 3D GO [21, 75, 76, 146–148].

3.2.5. Metal-free photocatalysts. Recently, a new class of photocatalyts known as metal-free photocatalysts have gained remarkable attention. These photocatalysts include selenium [149], red phosphorous [150, 151], carbon sulfide [152], boron carbides [153], graphitic carbon nitride [50, 154, 155], graphene quantum dots [69], and crystalline silicon [156]. Among these, graphitic carbon nitride (g-C_3N_4) and its nanocomposite have been believed to be the most promising ones for environmental applications like water and air purification [50, 157]. Figures 9(a) and (b) shows SEM images of g-C_3N_4 samples, as prepared by Xu [155]. g-C_3N_4 is constructed from s-triazine and tri-s-triazine planes that stack together in a structurally analogous way to graphene sheets in graphite [158]. It has high thermal stability (up to 600 °C in air) and resistance to chemical attacks, due to the highly condensed tri-s-triazine ring structure [158]. In addition to being non-toxic and easily processable, graphitic carbon nitride is a medium band-gap semiconductor (2.7 eV) and is excitable with visible light with wavelengths up to 470 nm. However, carrier mobility in g-C_3N_4 is restricted due to the absence of interlayer hybridization of the electronic states. Therefore, the photocatalytic activity of pure g-C_3N_4 is not sufficient for potential applications, which has led to significant efforts to improve its properties by doping and heterojunctions [157]. Table 5 summarizes these efforts by systematically comparing the photocatalytic efficiencies of different g-C_3N_4-based composites and nanocomposites. Note that the bulk composites are categorized as three-dimensional.

Recently, a novel g-C_3N_4 based nanocomposite has been developed by Zhang by combining g-C_3N_4 with carbon nanotubes and graphene [159]. It has been reported that g-C_3N_4 acts as an efficient photocatalyst whereas carbon nanotubes and graphene act as supercapacitors. This allows the nanocomposite to demonstrate post-illumination 'catalytic memory', which means that the photocatalyst can store a portion of its photocatalytic activity after illumination [159]. Another important metal-free photocatalyst is C_2N, which is another polymeric carbon nitride. It has been reported that layered C_2N possesses an optical band gap of as low as 1.96 eV [164]. In a recent study, the properties of single-layered (2D) C_2N and the effects of substitutional dopings have also been explored. The bandgap of monolayer C_2N has been reported to be 2.45 eV, which can be lowered to 2.01 with doping of boron [165].

3.2.6. Summary of recent progress on other nanomaterials. Other than the photocatalytic nanomaterials already discussed, many other nanomaterials have also been explored for water and wastewater treatment applications. They have been categorized here as oxide based and non-oxide type photocatalysts. Additionally, photocatalysts enhanced with polymers and hydrocarbons are particularly useful in the development of photocatalytic membranes. It should be noted that there is no sharp boundary between metal-free photocatalysts, carbon-based photocatalysts and hydrocarbon/polymer enhanced photocatalysts, and many photocatalytic materials can often be used interchangeably.

Other than the widely studied TiO_2, Fe_3O_4, and ZnO; tungsten trioxide (WO_3) and cuprous oxide (Cu_2O) are the most widely studied oxide type photocatalysts [166–171]. However, their photocatalytic performances are limited by their poor stability and rapid electron–hole recombination. Therefore, WO_3 and Cu_2O, being n-type and p-type semiconductors respectively, have been studied with many heterojunctions, particularly with rGO [168, 170]. However, in spite of their visible light activity, there is comparatively a limited amount of literature that endorses their potential for water and wastewater treatment applications.

Among the polymers, chitosan and polyaniline are the most widely used because of the presence of reactive amino groups, which enable the adsorption of several metal ions [172–174]. Polyaniline is also one of the best conducting polymers [173], whereas chitosan is mostly used as a support for MNPs because of its low cost, wide availability, biodegradability, non-toxicity, biodegradability and unique structural possessions [172].

Table 3. Various nanocomposites of TiO_2 for UV and Visible light photoactivity.

Composition	Light source	Pollutant	Experimental conditions	Dimensionality	PE	References
TiO_2	15 W UV	NO_x	$t_r = 16$ h	0D	25.4%	[33]
TiO_2 P25	250 W UV	Rhodamine B (10 mg l^{-1})	CL = 0.2 g l^{-1} $t_r = 60$ min	0D	55%	[17]
TiO_2	UV	Ammonia (700 mg l^{-1})	CL = N/A $t_r = 120$ min	0D	72%	[133]
TiO_2	125 W UV	*E. coli* (10^7 CFU/100 ml)	CL = 0.05-2 g l^{-1} $t_r = 10$ min	0D	72.22%–99.76%	[134]
N–TiO_2	300 W visible	Methylene blue	CL = 1 g l^{-1} $t_r = 240$ min	0D	~60%	[129]
Au doped TiO_2	24 W visible	Phenol (0.1 mM)	CL = 1 g l^{-1} $t_r = 240$ min	0D	74%	[117]
Al doped TiO_2	UV	Acid orange 7 (5 mg l^{-1})	CL = 0.5 g l^{-1} $t_r = 60$ min	0D	99%	[135]
S doped TiO_2	300 W UV	Methylene blue (10 mg l^{-1})	CL = 0.2 g l^{-1} $t_r = 12$ min	0D	95%	[24]
Ag doped TNH	UV–vis	Methylene Blue (30 mg l^{-1})	CL = 1 g l^{-1} $t_r = 15$ min	2D	~100%	[127]
N–TiO_2	Visible	*E. coli* (10^3 CFU ml^{-1})	CL = 0.5 g l^{-1} $t_r = 10$ min	3D	~100%	[130]
CdS-TNTA[a]	300 W visible	Rhodamine B (5 mg l^{-1})	CL = N/A $t_r = 300$ min	3D	68.14%	[4]
TiO_2 NRs-CNTs[b]	Sunlight	Methylene blue (5 mg l^{-1})	CL = 0.2 g l^{-1} $t_r = 180$ min	3D	97.5%	[72]

Note. PE = photodegradation efficiency.
CL = catalyst loading.
t_r = irradiation time.
TNH = TiO_2 nanoholes structure.
[a] TiO_2 nanotube arrays.
[b] TiO_2 nanoribbons and carbon nanotubes.

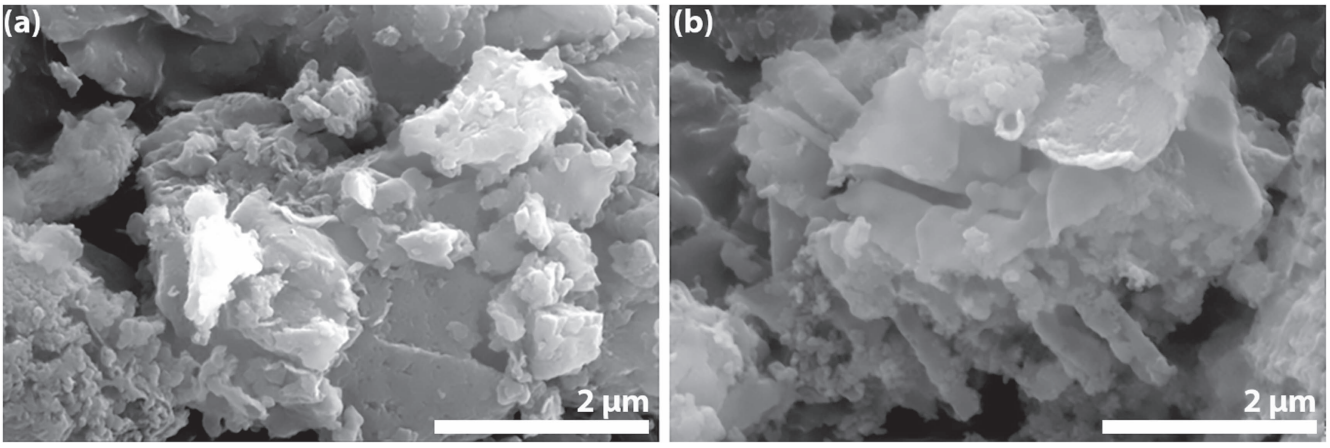

Figure 9. SEM images of g-C_3N_4 samples (Reprinted from Xu *et al* [155]. Licensed under Creative Commons Attribution 4.0 International License (http://creativecommons.org/licenses/by/4.0/). © 2015 Xu Gong et al.).

Table 4. Effect of graphene hybridization on the photocatalytic performance of TiO_2.

Composition	Light source	Pollutant	Experimental conditions	PE	References
TiO_2–GO	20 W UV	Methyl orange (10 mg l^{-1})	CL = 0.5 g l^{-1} t_r = 9 min	~90%	[140]
TiO_2–GO (10% GO)	Visible	Methyl orange (10 mg l^{-1})	CL = 1 g l^{-1} t_r = 3 h	62%	[141]
TiO_2–GO (20% GO)	Visible	Methylene blue (10 mg l^{-1})	CL = 0.8 g l^{-1} t_r = 100 min	98.8%	[85]
S–TiO_2–rGO	300 W UV	Methylene blue (10 mg l^{-1})	CL = 0.2 g l^{-1} t_r = 12 min	95%	[24]
TiO_2–rGO	15 W UV	NO_x	t_r = 16 h	42.86%	[33]
TiO_2–graphene	Visible	Methylene blue (10 mg l^{-1})	CL = 0.01 g l^{-1} t_r = 150 min	96%	[142]
MIP-TiO_2–graphene[a]	Visible	Bisphenol A (4 mg l^{-1})	CL = 1 g l^{-1} t_r = 180 min	67.6%	[139]
Co_3O_4–TiO_2–GO	300 W simulated sunlight	Congo red (10 mg l^{-1})	CL = 0.25 g l^{-1} t_r = 90 min	91%	[143]
TiO_2–Fe_3O_4–rGO	150 W Visible	TC-HCl (20 mg l^{-1})	CL = 20 mg l^{-1} t_r = 330 min	92.6%	[144]

Note. PE = photodegradation efficiency.
t_r = irradiation time.
CL = catalyst loading.
TC-HCl = tetracyclone hydrochloride.
[a] Molecular imprinted TiO_2-graphene nanocomposite prepared with bisphenol A and o-phenylenediamine.

Among the non-oxide type photocatalysts, zinc sulfide (ZnS) is a well-known photocatalyst, just like its oxide counterpart. Because of its wide-band gap energy (3.2–4.4 eV), a large exciton binding energy (40 meV), a small Bohr radius and high activity [175], it has gained intensive interests in phocotalysis [176, 177]. On the other hand, cadmium sulfide (CdS) is a narrow bandgap semiconductor, which makes it an attractive candidate for visible-light photocatalysis. Its narrow bandgap of 2.4 eV at room temperature, allows for an efficient absorption of visible light. Additionally, the band position of CdS semiconductor perfectly satisfies the thermodynamic requirements for photocatalytic dye degradation. Furthermore, the CB edge position of CdS is relatively more negative than that of the most studied semiconductors such as TiO_2 and ZnO, which indicates that the photogenerated electrons from CdS possess a stronger reducing power in the photocatalytic reactions [178].

Along with CdS and ZnS, table 6 systematically summarizes some recent nanocomposites other than previously discussed in this review. Many of these have shown an appreciable activity towards visible light, which makes them appreciable candidates for water and wastewater treatment applications, along with the previously discussed metal oxides and carbon-based photocatalytic materials. However, most of these materials currently do not have enough literature to support their potential for the aforementioned applications. Therefore, efforts are being made to explore possible heterojunctions and other variations to ensure their ability to photodegrade a broad spectrum of contaminants, in a wider variety of operating parameters.

3.3. Photocatalytic reactor design

A photocatalytic reactor for water or wastewater treatment can be as simple as the one shown in figure 10(a), which consists of TiO_2 coated glass beads and a UV lamp in the center [133]. However, in order to increase the irradiated surface area and to improve the efficiency, the photocatalytic reactors have been modified in many ways in the recent years.

Table 5. Photocatalytic performance of g-C_3N_4-based composites.

Composition	Light source	Pollutant	Experimental conditions	Dimensionality	PE	References
g-C_3N_4-CNTs-graphene	Visible	Phenol (5 mg l^{-1})	CL = 0.4 g l^{-1} t_r = 60 min	2D	43%	[159]
mpg-C_3N_4	300 W visible	4-Chlorophenol (15.4 mg l^{-1})	CL = 0.5 g l^{-1} t_r = 60 min	3D	~100%	[158]
g-C_3N_4–$BiVO_4$	30 W simulated sunlight	Methylene blue (10 mg l^{-1})	CL = 50 mg t_r = 70 min	3D	~68%	[160]
g-C_3N_4	Simulated sunlight	Methylene blue (5 mg l^{-1})	CL = N/A t_r = 120 min	3D	96.5%	[155]
g-C_3N_4–CDs[a]	300 W visible	Phenol (10 mg l^{-1})	CL = 1 mg l^{-1} t_r = 200 min	3D	87%	[161]
g-C_3N_4	300 W visible	Methylene blue (50 mg l^{-1})	CL = 1 g l^{-1} t_r = 5 h	3D	66%	[154]
g-C_3N_4–Ag–Fe_3O_4	300 W visible	Tetracycline (20 mg l^{-1})	CL = 0.5 g l^{-1} t_r = 90 min	3D	88%	[162]
g-C_3N_4–Fe_3O_4-BiOI	50 W visible	Rhodamine B (4.8 mg l^{-1})	CL = 0.4 g l^{-1} t_r = 180 min	3D	~100%	[163]

PE = photodegradation efficiency.
t_r = irradiation time.
CL = catalyst loading.
[a] Carbon dots.

Table 6. Summary of photocatalytic performance of other nanocomposites composites.

	Composition	Light source	Pollutant	Experimental conditions	Dimensionality	PE	References
Other metal oxide based photocatalysts	Cu_2O–rGO	400 W visible	Methylene blue (10 mg l^{-1})	CL = 0.33 g l^{-1} t_r = 120 min	2D	72%	[170]
	Cu_2O–$BiVO_4$	54 W visible	Methyl orange (10 mg l^{-1})	CL = 1 g l^{-1} t_r = 240 min	3D	89%	[169]
	WO_3–rGO	200 W visible	Sulfamethoxazole (10 mg l^{-1})	CL = 1 g l^{-1} t_r = 180 min	2D	>98%	[168]
	CeO_2–CdO	30 W UV	Malachite green (50 ppm)	CL = 0.3 g l^{-1} t_r = 60 min	2D	~100%	[179]
	Ag_3PO_4@ polyaniline	250 W visible	Phenol (10 mg l^{-1})	CL = 1 g l^{-1} t_r = 30 min	3D	~100%	[180]
Hydrocarbons/polymer-enhanced photocatalysts	Fe_3O_4-β-cyclodextrin	Sunlight	Bisphenol A (20 mg l^{-1})	CL = N/A t_r = 180 min	0D	82.5%	[181]
	ZnO-PMMA	UV	Methylene blue (4.8 mg l^{-1})	CL = 50 g l^{-1} t_r = 4 h	0D	~60%	[25-]
	Fe_3O_4–PVA @ PHB-PCL[a]	UV	Methylene blue (16 mg l^{-1})	CL = NFM t_r = 180 min	2D	~82%	[182]
	CuPc–rGO[b]	400 W visible	Rhodamine B (24 mg l^{-1})	CL = 0.25 g l^{-1} t_r = 210 min	1D	96.2%	[177]
	Polyaniline-ZnO	250 W visible	Methyl orange	CL = 1 g l^{-1} t_r = 180 min	0D	98.3%	[173]
	Chitosan–Cu–TiO_2	visible	Methyl orange (16.4 mg l^{-1})	CL = 7.1 g l^{-1} t_r = 15 min	0D	90%	[172]
	PAN–CNTs[c]	100 W UV	Indigo carmine (10 mg l^{-1})	CL = NFM t_r = 60 min	2D	~100%	[183]
Non-oxide type photocatalysts	CdS–gC_3N_4–rGO	350 W visible	Atrazine (10%)	CL = 0.44 g l^{-1} t_r = 300 min	2D	70.8%	[184]
	CdS–Bi_2S_3	300 W UV	Methyl red (10 mg l^{-1})	CL = 0.2 g l^{-1} t_r = 40 min	1D	~99%	[185]
	Cu–Au–ZnS	Solar Light	4-Nitrophenol (25 mg $^{l-1}$)	CL = 0.71 g l^{-1} t_r = 150 min	0D	62.9%	[186]
	SnS_2–rGO	150 W visible	Methl orange (9.82 mg l^{-1})	CL = 1 g l^{-1} t_r = 10 min	2D	91.7%	[187]
	AgI-BN	150 W simulated sunlight	Rhodamine B (10 mg l^{-1})	CL = 1 g l^{-1} t_r = 70 min	2D	96%	[188]
	ZnS	18 W visible	Methyl red (50 mg l^{-1})	CL = 0.5 g l^{-1} t_r = 120 min	0D	95.1%	[176]

Note. PE = photodegradation efficiency.
t_r = irradiation time.
NFM = nanofiber membranes.
CL = catalyst loading.
[a] Fe_3O_4- poly(vinyl alcohol) @ poly(3-hydroxybutyrate)-poly (ε-caprolactone).
[b] Copper Phthalocyanine—reduced graphene oxide.
[c] Polyacrylonitrile—carbon nanotubes.

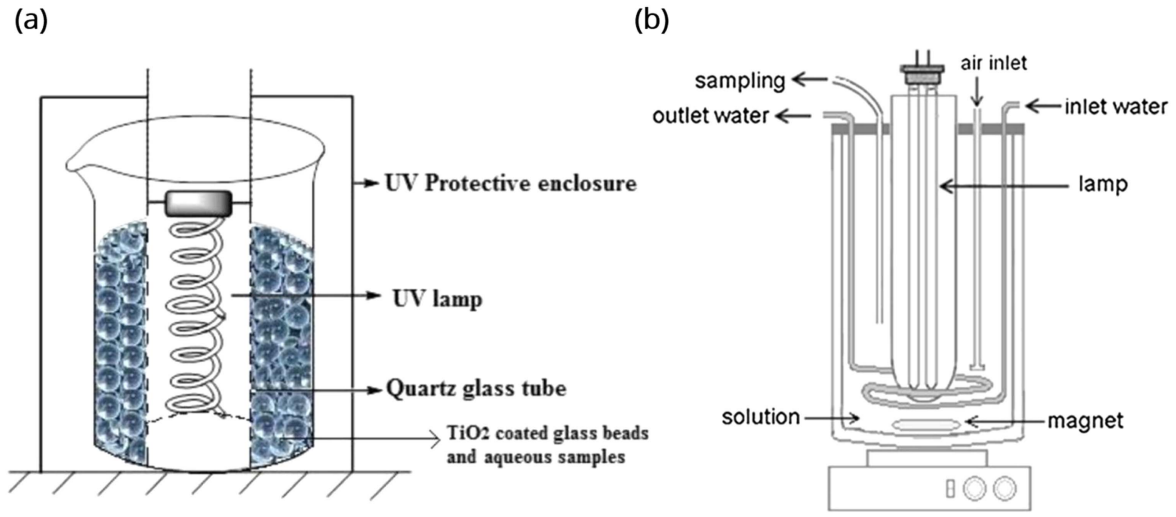

Figure 10. (a) A simple photocatalytic reactor which consists of TiO_2 coated glass beads and a UV lamp in the center. Reprinted by permission from Springer Nature Future Cities and Environment [133] Copyright 2015. (b) Configuration of a photocatalytic reactor proposed by Pirila. Reprinted by permission from Springer Nature Environmental Science and Pollution Research [191] Copyright 2014.

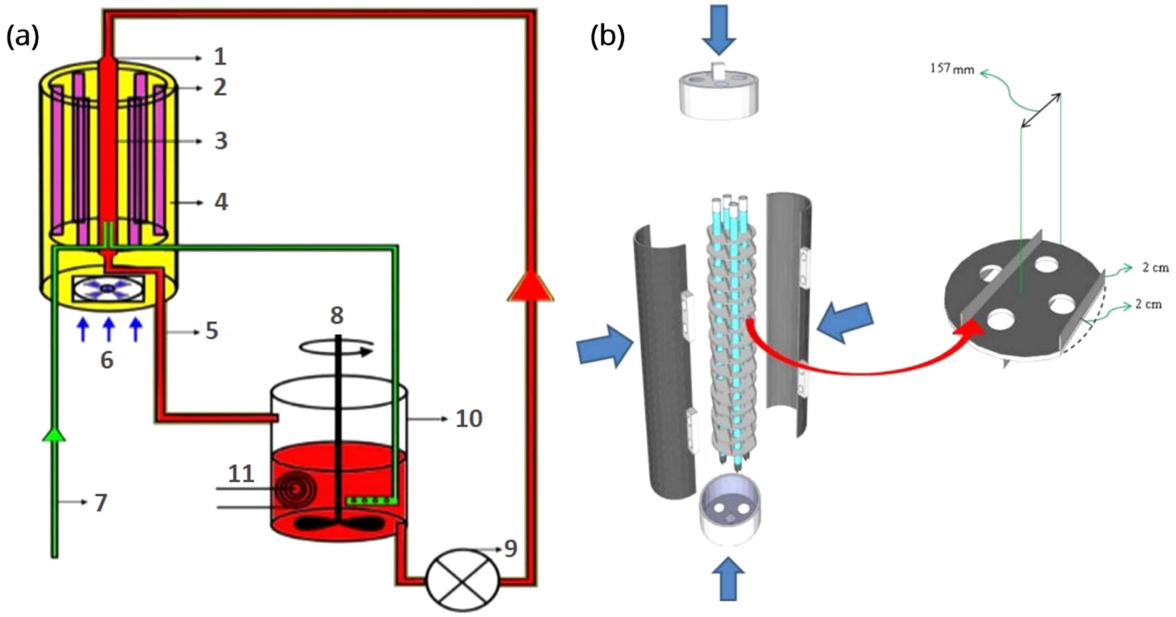

Figure 11. (a) Schematic of the laboratory-scale photocatalytic reactor developed by Abramovic: (1) liquid distributor; (2) UV lamps; (3) reactor column; (4) reflective insert; (5) pipe jacket; (6) ventilator; (7) air/O_2; (8) impeller mixer; (9) pump; (10) feed feed tank; (11) heater connected to the thermostat. (b) Dimension and arrangement of the photoreactor developed by Rezaei. Reprinted by permission from Springer Nature Environmental Science and Pollution Research [191] Copyright 2014.

A comparatively more complex design of a photocatalytic reactor, as proposed by Pirila, is illustrated in figure 10(b). This reactor consists of a Teflon vessel with a UV-A lamp enclosed in a quartz tube, fixed in the middle of the reactor cell. In this study, the irradiance in the annulus of the reactor was measured to be $52\,W\,m^{-2}$. The performance of the reactor was evaluated using four model pollutants which were diuron (herbicide), p-coumaric acid (agro-industrial wastewater), phthalic anhydride and bisphenol A (plasticizers). The initial concentration of the pollutants was $15\,mg\,l^{-1}$ and the experiments were done with a catalyst dose of $200\,mg\,l^{-1}$. Synthetic air was fed into the reactor and a constant agitation of the test solution was provided by a magnetic stirrer. It was concluded that, of the four pollutants, diuron was removed most efficiently while bisphenol A was found to be most difficult to be removed. However, it was found that the treatment of industrial wastewater matrix is much more difficult than the treatment of synthetic solution with this application. This is because the wastewater has a higher concentration of different contaminants, and they are presumably competing for the possible active sites on the catalyst materials [189]. This demands for a more efficient reactor

design with more active sites. It should be noted that the design configurations of photocatalytic reactors can be summarized into two types [42, 190]:

i. slurry type photocatalytic reactors;
ii. fixed bed type reactors.

Slurry type photocatalytic reactors utilize suspended photocatalyst particles which provides a higher contact area between the photocatalyst and the contaminated solution. Abramovic *et al* designed a similar reactor by using ZnO in a laminar falling film flurry in the reactor as shown in figure 11(a) [192]. The reactor consists of a set of six 18 W UV lamps, which can provide wavelengths up to 366 nm, enclosed in an aluminum housing. The lamps are arranged in a symmetrical way around the centered glass column. In order to prevent the external radiation, the pipes were placed in non-transparent plastic tubes, and the feed tank was placed in a wooden box in this study. The aqueous suspension of ZnO and thiacloprid insecticide in the feed tank was continuously stirred with an impeller mixer and the temperature was maintained at 25.0 °C ± 0.5 °C, using the additional air flow system. The suspension was circulated around the tank and the reactor column and it was concluded the rate of degradation increased with the increase in the ZnO loading and reached a plateau at a level of 2 g l^{-1}. However, after increasing the UV light intensity from 0.09 mW cm^{-2} to 1.75 mW cm^{-2} it was found that the degradation rate increased only two times because of the small volume of irradiated suspension [192]. Therefore, the total irradiated area of the semiconductor plays a crucial role in the efficiency of the photocatalytic reactor.

Contrary to slurry-type photoreactors, immobilized thin-film type photocatalytic reactors use a thin film photocatalyst either coated on the reactor walls, or coated on spherical glass beads, as shown in figure 10(a) [133]. The main difference between the slurry-type and immobilized configurations is that the former requires an extra separation and washing unit for the reclamation of the photocatalyst, while the latter allows a continuous operation. Additionally, the fixed-bed type reactors are usually continuous type, whereas, the slurry type reactors are batch-type in most configurations. Rezaei *et al* proposed a continuous flow immobilized TiO_2 reactor as shown in figure 11(b) [191]. This reactor consists of four quartz tubes enclosed in an aluminum tube. At the axis of the quartz tubes, four UV lamps with λ_{max} centered at 254 nm, are located. Twelve stainless steel circular baffles coated with TiO_2 nanoparticles are fixed inside the reactor. These baffles are arranged in a way to make zigzag pattern for liquid flow along the reactor length. The zigzag pattern provides a turbulent fluid flow in the reactor, and consequently provides high mass transfer coefficient inside the reactor. In this study, phenol was selected as a model pollutant to examine the performance of this novel photoreactor and the maximum predicted degradation of phenol was found to be 75.50% at the optimum processing conditions [191].

Other than the designs discussed above, there have been many other variations and improvements in the photocatalytic reactors. These modifications include a photocatalytic reactor proposed by Ziolli using high surface area colloid nanoparticles of TiO_2. Reference [44], and the photocatalytic membrane system developed by Molinari, by utilizing transparent Ca alginate/TiO_2 polymer fibers [193]. One of the main benefits of this type configuration is that it combines membrane separation and heterogeneous photocatalysis, both of which overcome the challenges of each other [194].

One of the key challenges in designing a photocatalytic reactor is to maximize the total irradiated surface area of the semiconductors [195]. Therefore, in fixed bed systems, the thickness of the supported photocatalytic layer should be thin enough to allow the semiconductor to be completely irradiated, thus improving the efficiency of the reactor. Studies have shown that the rate of photocatalysis is directly proportional to $\sqrt{I}$ at higher intensity and $I^{1.0}$ at comparatively low intensity [190]. Hence, the intensity is one of the most important features in photocatalytic reactor design, which is also directly related to the total irradiated surface area.

Another challenge in designing an efficient photocatalytic reactor, is the choice of the photocatalytic material. This depends mainly on the photocatalytic reactor configuration and its build-material. For example, TiO_2 and g-C_3N_4 are more suitable for fixed-bed type reactors because they can easily be immobilized by coating on substrates such as quartz [196], concrete [197], glass [198], Al_2O_3 [50],limestone [199] and polymers such as polyacrylonitrile [200], polyethyleneterephthalate [201] and pulysulfone [194]. On the other hand, Fe_3O_4-based nanomaterials aid with the magnetic separation, and reduce the cost associated with the additional separation unit. Therefore, Fe_3O_4-based photocatalysts can be more suitable for slurry-type photoreactors. However, Fe_3O_4 and ZnO are also emerging as promising candidates as the filler material in photocatalytic membrane reactors (PMRs) [182, 183, 202]. PMRs are hybrid fixed-bed type reactors which combine membrane separation with heterogeneous photocatalysis, and carry great potential for sustainable water and wastewater treatment [193].

3.4. Fundamental parameters

The efficiency of photocatalytic water or wastewater treatment, usually calculated in terms of removal efficiency [31], depends upon various parameters which will be discussed in this section. The removal efficiency (%) and equilibrium adsorbed concentration, q (mg g^{-1}) of the metal ions can be calculated by (1) and (2), where C_o and C_t are the initial and residual concentration of metal ions (mg l^{-1}) in aqueous solution, V is the total volume of solution (l) and M is the adsorbent mass (g) [31].

$$\text{Removal Efficiency } (\%) = \frac{(C_o - C_t)}{C_o} \times 100, \tag{8}$$

$$q = (C_o - C_t) \times \frac{V}{m} \tag{9}$$

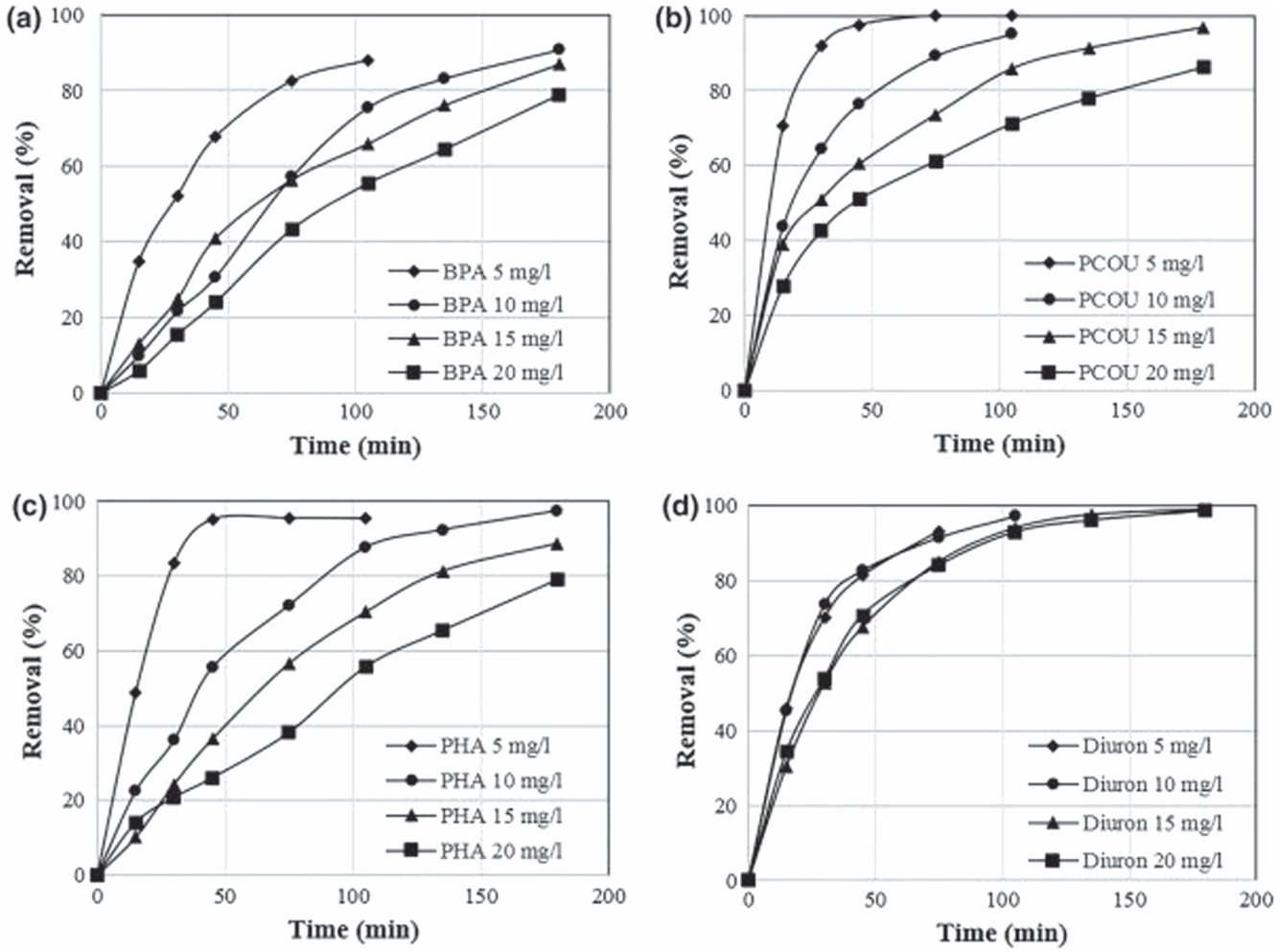

Figure 12. Removal of (a) bisphenol A (b) p-coumaric acid (c) pthalic anhydride and (d) diuron as a function of irradiation time with different initial concentrations.

3.4.1. Concentration of contaminants. It has been observed that, under similar operating conditions, change in the initial concentration of contaminants results in different irradiation time required to complete the disinfection or demineralization. Presence of excessive amount of contaminants reduces the overall process efficiency by saturating the TiO_2 surface [36, 42]. However, some organic substrates, such as oxalic acid, undergo direct transformation to carbon dioxide and water without the formation of intermediate compounds [42]. It should also be noted that increased contaminant concentration will act as a blocking surface between the incident photons and the catalyst [72].

In a study conducted by Pirila *et al* the degradation of four different model pollutants was studied over TiO_2 P25. The contaminants were diuron (herbicide), p-coumaric acid (found in agro-industrial wastewater), bisphenol A and phthalic anhydride (plasticizers). The results (illustrated in figure 12) indicate that the removal performance was affected as the concentration of contaminants was increased. When the concentration was increased to 20 mg l^{-1}, even 180 min of irradiation was not sufficient to completely remove the pollutants. However, diuron was not considerably affected by the initial concentration, and was effectively removed with all the tested initial concentrations [189]. Therefore, the dependency of the reaction rate on the contaminants' concentration depends strongly on the type of organic contaminants.

3.4.2. Temperature. Many studies have found that the photocatalytic reaction rate is strongly dependent on temperature [34, 36, 42]. Shen *et al* studied and compared the adsorption rates of Cu^{2+}, Cr^{6+}, Ni^{2+} and Cd^{2+} on Fe_3O_4 at different temperatures. In this study it was concluded that the adsorption rates of Cr^{6+}, Ni^{2+} and Cd^{2+} increased with temperature whereas the adsorption rate of Cu^{2+} was almost independent of temperature [63].

It has been observed that at temperatures above 80 °C, the adsorption of reactants on the TiO_2 surface is disfavored and the recombination of charge carriers is favored [34, 36, 42]. On the other hand, temperatures as low as 0 °C have been found to increase the apparent activation energy which limits the desorption of the final product [34]. Therefore, optimum reaction temperature for the reaction is reported to be in the range of 20 °C–80 °C.

3.4.3. pH. pH is one of the most significant operating parameters that affects the size of catalyst aggregates, charge

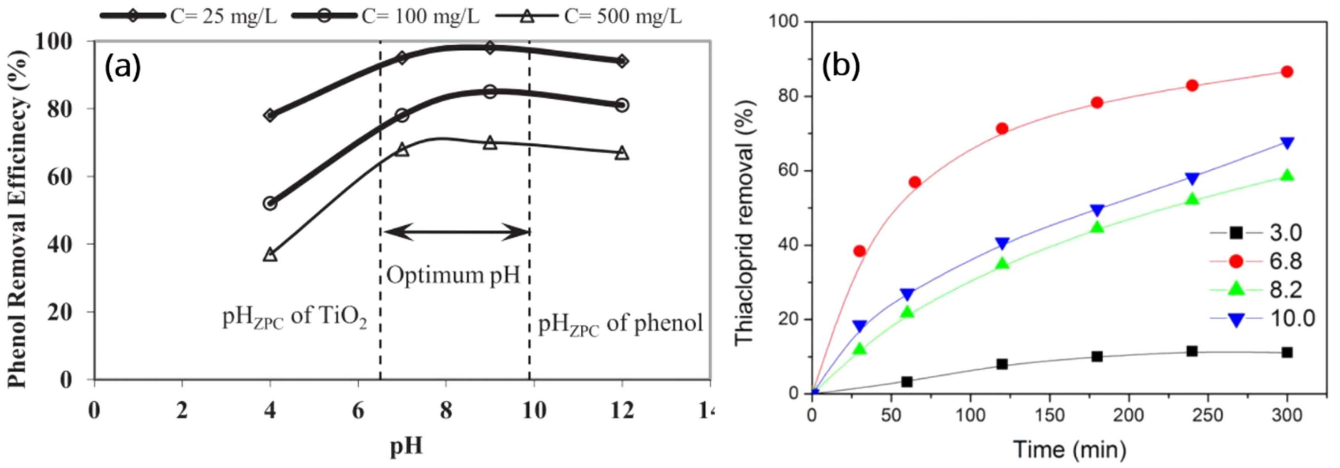

Figure 13. (a) Relationship of the phenol removal efficiency with pH at different loadings of TiO_2. (b) Removal rate of thiacloprid with ZnO at different pHs. Reprinted from [197]. Licensed under Creative Commons Attribution 4.0 International License (http://creativecommons.org/licenses/by/4.0/). © 2015 Delnavaz *et al.*

on the catalyst particles, and the position of conduction and valence bands [36, 42]. Many studies have reported a zero point charge (ZPC) pH value for TiO_2 which strongly affects its charge [34, 36, 42, 203, 204]. ZPC is the value at which the TiO_2 surface has no charge and hence the electrostatic attraction between the photocatalyst particles and water pollutants is minimal. If the pH of the aqueous solution is below the ZPC value, the TiO_2 surface becomes positively charged and exerts an electrostatic force towards the negatively charged compounds. On the other hand, if the pH is above the ZPC value, TiO_2 surface gets negatively charged and repels the anionic compounds in water, according to the following reactions [34, 42, 203]:

$$\text{At pH} < \text{ZPC: TiOH} + \text{H}^+ \leftrightarrow \text{TiOH}_2^+, \quad (10)$$

$$\text{At pH} > \text{ZPC: TiOH} + \text{OH}^- \leftrightarrow \text{TiO}^- + \text{H}_2\text{O} \quad (11)$$

The pH also affects the mean particle size of the TiO_2 aggregates. It has been observed that at pH close to the ZPC value, the particles become larger due to zero surface charge which inhibits the interactive rejection necessary to separate the particles [34]. For experiments with synthetic solutions such as p-toluidene, aniline, and 2,4-xylene, the TiO_2 has been found to be more effective in acidic and slightly alkaline media. However, in the case of the purification of ground water, a pH of 3.5 has been suggested as optimal for the degradation of phenol [28].

Figure 13(a) illustrates the relationship of pH with the phenol removal efficiency by different amounts of TiO_2 loading. The optimum pH reported in this study was approximately 6–10 for the catalyst loading of 25 mg l^{-1}, 100 mg l^{-1}, as well as 500 mg l^{-1} [197]. On the other hand, figure 13(b) shows the photocatalytic activity of ZnO for the removal of thiacloprid at the pH values of 3, 6.8, 8.2 and 10 [192]. The results suggest the pH of 6.8 gives much higher rate of thiacloprid removal than other experimental pH values. In case of Fe_3O_4, Shen has suggested an optimum pH of around 4.5 for Fe_3O_4 photocatalyst, for the optimum removal of toxic metal ions from wastewater, However, the adsorption rate of Cu^{2+} is almost independent of pH, just like it is independent of temperature as discussed before [63]. Therefore, pH is a very important parameter for the design of an effective water purification system.

3.4.4. Morphology of the photocatalyst. Photocatalysts with different morphologies generally do not display the same photocatalytic behavior due to the number of active facets, distinct active sites, and associated adsorption–desorption ability to reactant [61]. The photocatalytic behaviors of ZnO, TiO_2, graphene and Fe_3O_4 have been studied in different forms such as nanowires [42], nanorods [7, 42, 71, 114], nanocolumns [71], nanofibers [42] and nanoparticles [63, 68, 105, 111]. It has been reported that the photocatalytic activity is strongly dependent on the shape and size of the photocatalyst. Since the shape affects the surface area as well as the surface area to volume ratio, it affects the rate of reaction by minimizing or maximizing the contact area between the reactants and the photocatalyst. In general, smaller the particle size, the larger the surface area, and thus higher concentration of active sites per square meter [190]. It should also be noted that the dimensionality of the nanomaterials also plays a tremendous role in the overall reaction rate. For example, the superparamagnetic properties of Fe_3O_4 are optimized particularly in the form of zero-dimensional nanoparticles due to the finite size effect [62]. On the other hand, nanofibers have been reported to have an additional benefit that they can be commercially fabricated into microfilteration and ultrafilteration membranes [42].

3.4.5. Reaction time. The absorption or removal efficiency is strongly affected by the time of contact of the reactants as well as the irradiation time of the semiconductor. While studying the adsorption rates of various heavy metal impurities on Fe_3O_4 photocatalyst, it has been found that the adsorption rate is directly proportional to the contacting time [30, 63]. However, some pollutants such as Cu^{2+} and Cr^{6+}, have been found to adsorb readily as compared to Ni^{2+}

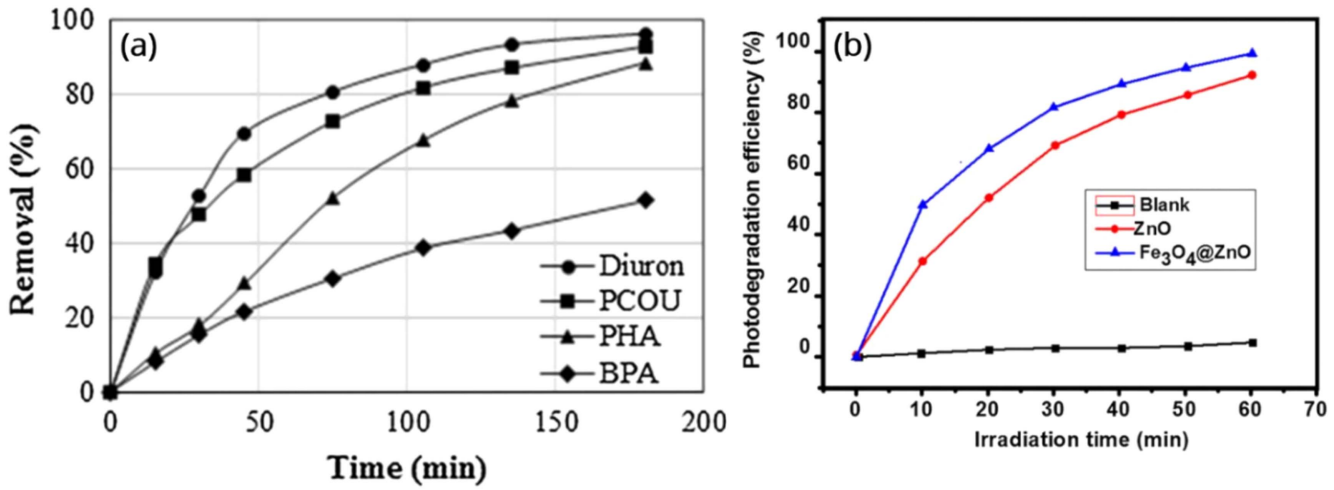

Figure 14. (a) Percentage removal of diuron, p-coumaric acid, bisphenol A and phthalic anhydride, as a function of irradiation time. Reprinted by permission from Springer Nature Environmental Science and Pollution Research [191] Copyright 2014. (b) Photodegradation efficiency of RhB by ZnO and Fe_3O_4–ZnO nanospheres. Reprinted by permission from Springer Nature Journal of Materials Science: Materials in Electronics [79] Copyright 2016.

and Cd^{2+}, which leads to the conclusion that in case of Ni^{2+} and Cd^{2+}, the rate of adsorption is more dependent on the contacting time.

Figure 14(a) demonstrates the relationship between the reaction time and percentage removal, as presented Pirila's study [189]. It is clear that the adsorption rates of of diuron, p-coumaric acid, bisphenol A and phthalic anhydride increase with time, with diuron showing the fastest removal rate, and bisphenol A showing the slowest. Similarly, figure 14(b) illustrates the photodegradation efficiency of RhB by ZnO and Fe_3O_4–ZnO nanospheres. The heterojunction of Fe_3O_4 and ZnO provides better photodegradation rate than pure ZnO [79]. This is presumably due to the increased concentration of surface oxygen vacancies. When designing a photocatalytic reactor, the reaction time should be carefully controlled in order to avoid excess cost associated with prolonged reaction cycles.

3.4.6. Amount of the photocatalyst. In most studies, it has been found that the overall photocatalytic reaction rate and removal efficiency is directly proportional to the amount of TiO_2 used [34, 42, 203]. This linear dependency continues up to a limiting value where the reaction rate becomes independent of the TiO_2 concentration. This limiting value depends upon the geometry and working conditions of the photoreactor, as well as on the total proportion of TiO_2 which is fully illuminated. Therefore the catalyst dose should be carefully adjusted in order to avoid excessive dosage, and thus reducing the overall cost of the treatment process [34, 36, 42].

3.4.7. Light wavelength and intensity. It has been reported that the initiation of photocatalytic reaction is not highly dependent on the intensity of light, since a few photons are adequate to induce a surface reaction. However, in order to achieve a high reaction rate, a comparatively higher light intensity is required to ensure the supply of sufficient photon energy on each TiO_2 active site. Thus, the wavelength and intensity of light have a significant effect on the photocatalytic reaction rate, and are affected by the type of photocatalysts used. In case of commercial Degussa P-25 TiO_2, a light wavelength of less than 380 nm has been reported to be sufficient [42]. However, with doping and modifications of P-25 TiO_2, the required wavelength of light can also be tailored [128].

3.4.8. Dissolved oxygen. Dissolved oxygen is one of the key parameters in TiO_2 photocatalysis as it contributes in the stabilization of radical intermediates, direct photocatalytic reactions as well as mineralization. It also ensures the presence of sufficient electron scavengers for the prevention of recombination of charge carriers, by trapping the photo-generated electrons. Additionally, DO also provides adequate buoyant force in photocatalytic reactors for the complete suspension of TiO_2 particles [42]. The overall reaction involving the photo-mineralization of organic pollutants can be summarized by the given equation [34, 36].

$$\text{organic pollutant} + O_2 \xrightarrow{\text{ultrabandgap energy}} CO_2 + H_2O + \text{mineral acids} \quad (12)$$

Hence, there will be no photo-mineralization unless oxygen is present [36].

3.5. Improving the photocatalytic efficiency

The photocatalytic performance can be expressed in terms of quantum yield, which can be defined as the ratio between the reaction rate and the photonic flux, i.e. as the ratio of the number of molecules degraded per second to the number of

incident efficient photons per second [205]. Mathematically,

$$\text{quantum yield} = \frac{\text{number of molecules degraded/transformed}}{\text{number of incident photons}}. \quad (13)$$

One of the main drawback with TiO_2 solar photocatalysis is the electron/hole recombination, which is accompanied by the dissipation of energy in the form of heat, consequently decreasing the efficiency of the process as well as affects the quantum yield. In the absence of proper electron acceptors, this is a major energy-wasting step. Using oxygen as an electron scavenger solves this problem upto some extent but gives low mineralization photo-efficiency [34].

Although TiO_2 photocatalysis shows high activity and stability under UV light, but it only comprises 5% of the solar spectrum. In order to increase the photo-efficiency of the process, the photocatalyst should be made capable to utilize the visible spectrum. Various strategies have been adopted to solve these problems which include [34]:

- Using chemical oxidants.
- Doping and modifying the TiO_2 surface.
- Using photosensitizers coupled with TiO_2 photosynthesis.
- Combining semiconductor photocatalysis with other AOPs [34].

3.5.1. Chemical oxidants. Chemical oxidants such as hydrogen peroxide, peroxodisulphate, chlorate and bromate can prevent electron–hole recombination by adding electron acceptors to the reaction. This is because the addition of oxidants increases the number of trapped electrons [34, 206]. Oxidants also generate more ·OH radicals and other oxidizing species. Additionally, the oxidation rate of intermediate compounds is also increased by the addition of oxidants. Moreover, the oxygen supply for the reaction may sometimes be inadequate, due to either oxygen consumption or slow mass transfer of oxygen. Such problems caused by the O_2 starvation can also be prevented by the addition of oxidants like hydrogen peroxide. However, the oxidant should be able to eventually dissociate into harmless compounds [34, 206].

3.5.2. Doping and modifying the semiconductor surface. Pure and unmodified TiO_2 works at mild conditions with mild oxidants, at utilizes only the UV spectrum. However, at higher concentration of contaminants, the process gets complicated and challenging due to catalyst deactivation, slow kinetics, and low photo-efficiencies. In order to use unmodified TiO_2 for practical applications such as the treatment of industrial and environmental effluents, artificial light has to be employed which adds to the cost of the overall process [34].

However, this high cost can be avoided and the catalyst deactivation can be prevented by modifying or doping TiO_2 with nitrogen, sulfur, copper or noble metals. During last few years, transitional metal ion doping has also been proven very useful.

Another way of modifying TiO_2 for photocatalysis is by coupling it with another semiconductor with a smaller bandgap, as discussed before. This can be achieved only when [34]:

- The small bandgap semiconductor is able to be excited by visible light.
- Both semiconductors are photocorrosion free.
- Electron injection is fast and efficient.
- The CB of the smaller band gap semiconductor is more negative than the large band gap semiconductor [34].

3.5.3. Photosensitizers. Dyes having redox ability and visible light sensitivity can be used with TiO_2 for the energy conversion of visible light. These dyes, when excited, can inject electrons to the CB of semiconductors to initiate the catalytic reactions under visible light illumination. In such system, the dye, instead of the photocatalyst, absorbs the light and gets photo-excited. This is important considering that the industrial textile waste water consists a large amount of dyes [34, 207]. Moreover, in many studies graphene and carbon nanotubes are reported to behave as photosensitizers under visible light [33, 208, 209]. Sensitized photocatalysis typically causes rapid destruction of chromophore structure into smaller organic species, leading to the final mineralization of the dye [34].

3.5.4. Combining semiconductor photocatalysis with other AOPs. The photocatalytic efficiency can be greatly enhanced by coupling semiconductor photocatalysis with other processes such as ozone treatment, vacuum ultraviolet treatment, or using hybrid processes such as PMRs, as discussed before in section 3.2.6 [34, 193, 210]. Kertèsz studied a low pressure microfilteration system to find the optimal conditions for a PMR by using hollow fibers, and to separate and recover the photocatalyst post-treatment [211]. Papageorgiou did the same by using Ca alginate fibers which provide an additional benefit of being transparent [3]. However, fouling of the membrane by impurities is one possible drawback of this hybrid technology, which may often result in an increased pressure drop or a decrease in the permeate flux. Similarly, Gebregiogis combined heterogeneous photocatalysis with biological oxidation and carried out a successful 90% discoloration of real textile wastewater by using TiO_2 powder as the photocatalyst [212].

3.6. Recyclability

In order to implement heterogeneous photocatalysis into practical water and wastewater treatment applications, the overall cost of the process should be minimized. One of the ways to decrease the cost is to improve the recyclability of the photocatalyst. Many TiO_2 and g-C_3N_4 based photocatalysts have been studied for recyclability. For example, in a study conducted by Hong, a V_2O_5–C_3N_4 photocatalyst has been tested for recyclability. It has been reported that the composite shows no apparent deactivation even after 5 cycles [82]. Similarly, polyacrylonitrile fibers coated with TiO_2 have been reported to show excellent dye removal after several

cycles [200]. However, some amount of the photocatalyst is lost by the water currents after every cycle. As a result, many efforts have been made to further enhance the recyclability, which involve either of the following approaches:

- Immobilizing the photocatalyst.
- Making more efficient PMRs.
- Using magnetic photocatalysts

3.6.1. Immobilized photocatalysts. One of the main advantages of TiO_2 is that it can easily be immobilized by coating on a substrate such as quartz [196], glass [196], concrete [197], or transparent fluorine-doped tin oxide [70]. Similarly, the immobilization of g-C_3N_4 on Al_2O_3 substrate has been reported to be useful for the visible light photocatalytic removal of NO [50]. More interestingly, She *et al* recently developed a novel Au–ZnO–rGO foam that can be used as a self-standing recyclable photocatalyst. This 3D nanocomposite can be directly employed as an immobilized photocatalyst in recyclable photodegradation [21]. As discussed in section 3.4, immobilization helps to decrease the cost of the overall process by eliminating the separation and recovery chamber, but decreases the contact area between the photocatalyst and the reactants, consequently compromising the efficiency.

3.6.2. Photocatalytic membranes. One of the most critical limitations of conventional polymeric and ceramic membranes is that they can be fouled easily. Photocatalytic membranes have been reported to have better fouling resistance, as well as antimicrobial properties. Such membranes can be developed by assembling the nanomaterials into MF and NF membranes in different ways, which include assembling the nanoparticles into ultra-thin membranes, or fabricating a membrane with nanofibers or aligned nanotubes [213]. Two-dimensional nanosheets like graphene have also been reported to be useful for membrane applications [136]. Additionally, combination of nanowires with graphene sheets has also gained attention recently. Such type of structure provides anti fouling and antimicrobial properties, as well as hydrophilicity and aqueous stability [213–215]. In some studies, Fe_3O_4 and TiO_2 nanoparticles have also been successfully used as a filler for composite membranes [216, 217]. Hence, nanomaterials open a broad spectrum of recycling possibilities in the form of MF and NF membrane applications.

3.6.3. Magnetic photocatalysts. Another way to ensure the recyclability of the photocatalyst is to introduce a magnetic constituent into the photocatalytic nanocomposite. Thus, the photocatalyst can be magnetically recovered post treatment by the application of an external magnetic field. Additionally, the incorporation of magnetic components can also prevent the agglomeration of the photocatalyst particles during recovery. Fe_3O_4 is the most widely used magnetic material, and has been successfully used in core–shell configurations with ZnO [79, 102], TiO_2 [17], β-cyclodextrin [181] and Bi_2O_3 [105]. However, magnetic separation involves an additional time-consuming separation process, which limits the continuous flow of the photocatalytic reactor. Hence magnetic separation would be more suitable for batch-type processes.

3.7. Life cycle assessment

In order to implement these photocatalytic processes on a large scale, a life cycle assessment (LCA) is necessary. LCA is one of the most useful tools for the assessment of the environmental impacts of a process, as well its feasibility and the costs involved. Current literature contains a lot of information about the recyclability and reusability of these semiconductor photocatalysts [42, 203, 218]. Matthews studied the recyclability of TiO_2 by using the photocatalyst again and again and found almost the same removal efficiency after 20 passes. However, the efficiency of the photocatalytic process is strongly dependent on the quality of feedwater and preliminary cleaning treatments too. In another study, a LCA has been carried out for various AOPs including heterogeneous photocatalysis for the treatment of kraft mill bleaching wastewaters. It has been reported that the environmental impact is mainly caused by the amount of electricity consumed, is barely affected by the production of the photocatalysts [219]. This is one of the reasons why so much research has been devoted to solar photocatalysis in the past decade.

Using LCA, the environmental impacts and waste discharges of a product can be individually identified and minimized. Some studies have been conducted in this regard [42] and a few pilot plants have been established to obtain the required data, such as the ones located at the PSA (Plataforma Solar de Almeria, Spain) and INETI (Instituto Nacional de Engenharia, Technologia Industrial e Inovaco, Portugal). One of these studies, in which α-methyl-phenylglycine has been used as a target contaminant, suggests that heterogeneous photocatalysis requires a larger solar collector area than homogeneous photo-Fenton process, in order to provide the same amount of efficiency. However, compared to existing biological wastewater treatment techniques, it can still lower the eutrophication potential [220]. With research and exploration of more photoactive materials, it is possible to overcome the existing constraints and allow the expansion of this technology to industrial scale.

3.8. Photocatalysis on real water samples

In the last two years, considerable efforts have been made to utilize heterogeneous photocatalysis for real water samples [221]. Some of the most successful efforts involve combining heterogeneous photocatalysis with coagulation-flocculation [29], heterogeneous photo-Fenton [222] or biological oxidation [212]. However, as a stand-alone water treatment technique, this process still faces some limitations related to the operating parameters, which have been discussed in section 3.4.

In a study conducted by Booshehri *et al* an Ag–$BiVO_4$ nanocomposite has been used successfully for the inactivation of pathogens in well water as well in in the secondary

effluents from municipal water. It has been reported that the high concentrations of carbonates and bicarbonates in the well water does not affect the photocatalytic efficiency. However, the natural organic matter in the secondary effluents limited the process efficiency due to the competitiveness for the radicals generated [223]. In another study by Ye *et al* TiO_2 nanotube arrays have been tested for the removal of metoprolol from synthetic solutions as well as from tap water. It has been reported that the photocatalytic efficiency reduced from 87% to 62% when using tap water [224]. Similarly, Deng *et al* used Ag modified phosphorous doped gC_3N_4–$BiVO_4$ nanocomposite for the removal of ciprofloxacin. In his study, the solutions have been made in actual lake water in order to study the photocatalytic efficiency in natural conditions, and a 92.6% efficiency has been obtained [225]. However, it cannot be neglected that the process becomes more challenging in real situations because of the varying types and concentrations of contaminants.

4. Future challenges and prospects

One of the key features for heterogeneous photocatalysis to be such a promising water treatment method, is that it can run at ambient temperature and pressure, utilizing atmospheric oxygen as oxidant. Furthermore, this process can be applicable to a variety of hazardous contaminants, ranging from organic contaminants such as pesticides, herbicides and detergents; to industrial contaminants such as dyes and toxic metal ions. However, after almost 30 years of extensive research and thorough studies of hundreds of photocatalytic semiconductors, there are still many aspects of this process that need to be addressed before its commercial implementation.

First, it should be determined whether the photocatalytic process should be used as a pre-treatment process or a stand-alone water purification technique. If used as a stand-alone technique, with current advancements, the required reaction time would still be much longer due to the slow kinetics of the reaction.

The second most important challenge is to eliminate the constraints related to operating parameters. Since the chemical composition and pH of industrial wastewater varies from region to region, efforts should be made for the development of photocatalytic materials which can be useful in a wide range of operating conditions such as temperature, pH and contaminant concentrations. For this purpose, a lot of research should be dedicated for the doping and modifications of TiO_2 as well as other semiconductors in order to achieve continuous irradiation with visible light, at a wider range of operating conditions. Another challenge comes in terms of catalyst immobilization strategy, which should be optimized in order to obtain maximum irradiated surface area of the photocatalyst. Catalyst immobilization is necessary to avoid the problems associated with catalyst recovery and agglomeration, which is a great issue in slurry-based photoreactors. Moreover, catalyst immobilization can also reduce the scale of the reactor by eliminating the separation and washing unit.

To answer the above concerns, more research should be focused on visible-light driven photocatalysis, as well as the phocatalytic reactor design in the coming years. Visible light-driven water treatment processes offer great potential to replace the conventional water and wastewater treatment techniques by offering a sustainable and environment-friendly alternative. As discussed in section 3.5, there are many ways to enhance the visible-light activity of semiconductors. It is suggested that doping and photosensitization are two of the most promising techniques for the future. Additionally, doping semiconductors with noble metals like gold or silver has been proven to be an efficient way to improve the visible-light activity of the semiconductors. A significant problem that still needs to be addressed is preventing the electron–hole recombination in the photocatalytic nanomaterials. Although semiconductor-graphene heterojunctions have contributed a lot to solve this issue, there is still a need for improving these heterojunctions for a more effective charge separation. It should also be noted that combining heterogeneous photocatalysis with other AOPs may not contribute a lot towards visible light activity, but it has a lot of potential for increasing the time efficiency of the process. Other than the visible light activity, effective design of photocatalytic reactor systems is also required, which can provide cost-effective, sustainable, and flexible alternative to the conventional water and wastewater treatment processes.

In terms of photocatalytic reactor design, the future design trends may find the continuous or fixed- bed type reactors more useful, as well as time and cost-efficient. So far, there have been two most efficient ways to increase the performance of continuous processes; one of them is to combine heterogenous photocatalysis with membrane processes (PMRs), and the other one is to maximize the contact time between the solution and the immobilized photocatalyst. The photocatalytic reactor shown in figure 11(b) is an example of the latter. Additionally, such helical tube type photoreactors utilize the minimum land area, and thus are more economical. Therefore, it is suggested that the future research should be comparatively more inclined towards the development of multi-stage PMRs and highly efficient fixed-bed-type reactors. In case of fixed-bed type reactors, efforts should be made to increase the turbulence of water flow as well. If the current limitations are overcome, heterogeneous photocatalysis can be employed as a sustainable process for the treatment of water and wastewater in the upcoming decades and may provide a cheap and environment-friendly solution for coping with the rising demands of water globally.

5. Conclusion

Heterogeneous photocatalysis has been proven to carry significant potential for the degradation of organic compounds, bacteria and microorganisms, as well as the reduction of toxic metal ions present in water and wastewater. The environmentally friendly nature of this technique makes it a

promising candidate for these applications. Furthermore, many photocatalytic materials have been studied on various potential contaminants in the past three decades, and some of them have been proven useful in visible light too. However, so far, this technique has mainly been studied in laboratories, and not appreciably implemented in industries. It is suggested that the future studies should not only focus on the materials, but also on the photocatalytic reactor design. By optimizing the photocatalytic reactor design, this technique can overcome the remaining challenges associaby nearly one-thirdted with it.

Acknowledgments

The authors would like to acknowledge Zia Ur Rahman, Hassnain Asgar and Dr Ali Nemati for reviewing this paper and providing their feedbacks.

Conflict of interest disclosure

The authors declare no conflict of financial interest.

ORCID iDs

Syed Nabeel Ahmed https://orcid.org/0000-0003-2070-4841
Waseem Haider https://orcid.org/0000-0003-4235-3560

References

[1] UNESCO 2018 *The United Nations World Water Development Report 2018: Nature-Based Solutions for Water*
[2] Vereb G, Manczinger L, Oszko A, Sienkiewicz A, Forro L, Mogyorosi K, Dombi A and Hernadi K 2013 Highly efficient bacteria inactivation and phenol degradation by visible light irradiated iodine doped TiO_2 *Appl. Catal.* B **129** 194–201
[3] Papageorgiou S K, Katsaros F K, Favvas E P, Romanos G E, Athanasekou C P, Beltsios K G, Tzialla O I and Falaras P 2012 Alginate fibers as photocatalyst immobilizing agents applied in hybrid photocatalytic/ultrafiltration water treatment processes *Water Res.* **46** 1858–72
[4] Zhu Y *et al* 2015 Visible light induced photocatalysis on CdS quantum dots decorated TiO_2 nanotube arrays *Appl. Catal.* A **498** 159–66
[5] Yue Z, Liu A, Zhang C, Huang J, Zhu M, Du Y and Yang P 2017 Noble-metal-free hetero-structural CdS/Nb_2O_5/N-doped-graphene ternary photocatalytic system as visible-light-driven photocatalyst for hydrogen evolution *Appl. Catal.* B **201** 202–10
[6] Das T, Rocquefelte X, Laskowski R, Lajaunie L, Jobic S, Blaha P and Schwarz K 2017 Investigation of the optical and excitonic properties of the visible-light driven photocatalytic $BiVO_4$ material *Chem. Mater.* **29** 3380–6
[7] Rodríguez J, Paraguay-Delgado F, López A, Alarcón J and Estrada W 2010 Synthesis and characterization of ZnO nanorod films for photocatalytic disinfection of contaminated water *Thin Solid Films* **519** 729–35
[8] Rajendran S, Khan M M, Gracia F and Qin J 2016 Ce^{3+}-ion-induced visible-light photocatalytic degradation and electrochemical activity of ZnO/CeO_2 nanocomposite *Sci. Rep.* **6** 1–11
[9] Shu J, Wang Z, Xia G and Zheng Y 2014 One-pot synthesis of AgCl @ Ag hybrid photocatalyst with high photocatalytic activity and photostability under visible light and sunlight irradiation *Chem. Eng. J.* **252** 374–81
[10] Yang S-F, Niu C-G, Huang D-W, Zhang H, Liang C and Zeng G-M 2017 $SrTiO_3$ nanocubes decorated with Ag/AgCl nanoparticles as photocatalysts with enhanced visible-light photocatalytic activity towards the degradation of dyes, phenol and bisphenol A *Environ. Sci. Nano* **4** 585–95
[11] Isaifan R J, Samara A, Suwaileh W, Johnson D and Yiming W 2017 Improved self-cleaning properties of an efficient and easy to scale up TiO_2 thin films prepared by adsorptive self-assembly *Sci. Rep.* **7** 1–9
[12] Yang X, Chen W, Huang J, Zhou Y, Zhu Y and Li C 2015 Rapid degradation of methylene blue in a novel heterogeneous photo-Fenton system *Sci. Rep.* **5** 1–10
[13] Mascolo M C, Pei Y and Ring T A 2013 Room temperature co-precipitation synthesis of magnetite nanoparticles in a large ph window with different bases *Materials* **6** 5549–67
[14] Upadhyay S, Parekh K and Pandey B 2016 Influence of crystallite size on the magnetic properties of Fe_3O_4 nanoparticles *J. Alloys Compd.* **678** 478–85
[15] Han L, Li Q, Chen S, Xie W, Bao W, Chang L and Wang J 2017 A magnetically recoverable Fe_3O_4–NH_2–Pd sorbent for capture of mercury from coal derived fuel gas *Sci. Rep.* **7** 2–11
[16] Bagbi Y, Sarswat A, Mohan D, Pandey A and Solanki P R 2017 Lead and chromium adsorption from water using L-cysteine functionalized magnetite (Fe_3O_4) nanoparticles *Sci. Rep.* **7** 1–15
[17] Chen Y, Yuan T, Wang F, Hu J and Tu W 2016 Magnetically separable Fe_3O_4@TiO_2 nanospheres: preparation and photocatalytic activity *J. Mater. Sci., Mater. Electron.* **27** 9983–8
[18] Han S, Yu H, Yang T, Wang S and Wang X 2017 Magnetic activated-ATP@Fe_3O_4 nanocomposite as an efficient fenton-like heterogeneous catalyst for degradation of ethidium bromide *Sci. Rep.* **7** 1–12
[19] Masih D, Ma Y and Rohani S 2017 Graphitic C_3N_4-based noble-metal-free photocatalyst systems: a review *Appl. Catal.* B **206** 556–88
[20] Feng Y, Wang G, Liao J, Li W, Chen C, Li M and Li Z 2017 Honeycomb-like ZnO mesoporous nanowall arrays modified with Ag nanoparticles for highly efficient photocatalytic activity *Sci. Rep.* **7** 1–11
[21] She P, Yin S, He Q, Zhang X, Xu K, Shang Y, Men X, Zeng S, Sun H and Liu Z 2017 A self-standing macroporous Au/ZnO/reduced graphene oxide foam for recyclable photocatalysis and photocurrent generation *Electrochim. Acta* **246** 35–42
[22] Silva C G and Faria J L 2016 Ag-loaded ZnO materials for photocatalytic water treatment *Chem. Eng. J.* **318** 95–102
[23] Novoselov K S, Geim A K, Morozov S V and Jiang D 2004 Electric field effect in atomically thin carbon films *Science* **306** 666–9
[24] Wang W, Wang Z, Liu J, Luo Z, Suib S L and He P 2017 Single-step one-pot synthesis of TiO_2 nanosheets doped with sulfur on reduced graphene oxide with enhanced photocatalytic activity *Sci. Rep.* **7** 1–9
[25] Di Mauro A, Cantarella M, Nicotra G, Pellegrino G, Gulino A, Brundo M V, Privitera V and Impellizzeri G 2017 'Novel synthesis of ZnO/PMMA nanocomposites for photocatalytic applications *Sci. Rep.* **7** 1–12

[26] Solomon R V, Lydia I S, Merlin J P and Venuvanalingam P 2012 Enhanced photocatalytic degradation of azo dyes using nano Fe_3O_4 *J. Iran. Chem. Soc.* **9** 101–9

[27] Carré G, Hamon E, Ennahar S, Estner M, Lett M C, Horvatovich P, Gies J P, Keller V, Keller N and Andre P 2014 TiO_2 photocatalysis damages lipids and proteins in *Escherichia coli Appl. Environ. Microbiol.* **80** 2573–81

[28] Kabra K, Chaudhary R and Sawhney R L 2004 Treatment of hazardous organic and inorganic compounds through aqueous-phase photocatalysis: a review *Ind. Eng. Chem. Res.* **43** 7683–96

[29] Ayekoe C Y P, Robert D and Lancine D G 2017 Combination of coagulation-flocculation and heterogeneous photocatalysis for improving the removal of humic substances in real treated water from Agbo River (Ivory-Coast) *Catal. Today* **281** 2–13

[30] Li J, Zhang S, Chen C, Zhao G, Yang X, Li J and Wang X 2012 Removal of Cu(II) and fulvic acid by graphene oxide nanosheets decorated with Fe_3O_4 nanoparticles *ACS Appl. Mater. Interfaces* **4** 4991–5000

[31] Singh S, Barick K C and Bahadur D 2013 Fe_3O_4 embedded ZnO nanocomposites for the removal of toxic metal ions, organic dyes and bacterial pathogens *J. Mater. Chem.* A **1** 3325

[32] Fujishima A and Honda K 1972 Electrochemical photolysis of water at a semiconductor electrode *Nature* **238** 37–8

[33] Trapalis A, Todorova N, Giannakopoulou T, Boukos N, Speliotis T, Dimotikali D and Yu J 2016 TiO_2/graphene composite photocatalysts for NOx removal: a comparison of surfactant-stabilized graphene and reduced graphene oxide *Appl. Catal.* B **180** 637–47

[34] Malato S, Fernandez-Ibanez P, Maldonado M I, Blanco J and Gernjak W 2009 Decontamination and disinfection of water by solar photocatalysis: Recent overview and trends *Catal. Today* **147** 1–59

[35] Low J, Yu J, Jaroniec M, Wageh S and Al-Ghamdi A A 2017 Heterojunction photocatalysts *Adv. Mater.* **29** 1601694

[36] Malato S, Maldonado M I, Fernández-Ibáñez P, Oller I, Polo I and Sánchez-Moreno R 2016 Decontamination and disinfection of water by solar photocatalysis: the pilot plants of the Plataforma Solar de Almeria *Mater. Sci. Semicond. Process.* **42** 15–23

[37] Srikanth B, Goutham R, Narayan R B, Ramprasath A, Gopinath K P and Sankaranarayanan A R 2017 Recent advancements in supporting materials for immobilised photocatalytic applications in waste water treatment *J. Environ. Manage.* **200** 60–78

[38] Spasiano D, Marotta R, Malato S, Fernandez-Ibanez P and Di Somma I 2015 Solar photocatalysis: materials, reactors, some commercial, and pre-industrialized applications. A comprehensive approach *Appl. Catal.* B **170–171** 90–123

[39] Byrne J A, Dunlop P S M, Hamilton J W J, Fernandez-Ibanez P, Polo-Lopez I, Sharma P K and Vennard A S M 2015 A review of heterogeneous photocatalysis for water and surface disinfection *Molecules* **20** 5574–615

[40] Shiraishi F and Ishimatsu T 2009 Toluene removal from indoor air using a miniaturized photocatalytic air purifier including a preceding adsorption/desorption unit *Chem. Eng. Sci.* **64** 2466–72

[41] Dong F, Ou M, Jiang Y, Guo S and Wu Z 2014 Efficient and durable visible light photocatalytic performance of porous carbon nitride nanosheets for air purification *Ind. Eng. Chem. Res.* **53** 2138–40

[42] Chong M N, Jin B, Chow C W K and Saint C 2010 Recent developments in photocatalytic water treatment technology: a review *Water Res.* **44** 2997–3027

[43] Zhao Z, Tian J, Sang Y, Cabot A and Liu H 2015 Structure, synthesis, and applications of TiO_2 nanobelts *Adv. Mater.* **27** 2557–82

[44] Ziolli R L and Jardim W F 2001 Photocatalytic decomposition of seawater-soluble crude oil fractions using high surface area colloid nanoparticles of TiO_2 *J. Photochem. Photobiol.* A **5887** 1–8

[45] Vela N, Martínez-Menchón M, Navarro G, Pérez-Lucas G and Navarro S 2012 Removal of polycyclic aromatic hydrocarbons (PAHs) from groundwater by heterogeneous photocatalysis under natural sunlight *J. Photochem. Photobiol.* A **232** 32–40

[46] King S M, Leaf P A, Olson A C, Ray P Z and Tarr M A 2014 Photolytic and photocatalytic degradation of surface oil from the Deepwater Horizon spill *Chemosphere* **95** 415–22

[47] da Rocha O R S, Dantas R F, Duarte M M M B, Duarte M M L and da Silva V L 2010 Oil sludge treatment by photocatalysis applying black and white light *Chem. Eng. J.* **157** 80–5

[48] Rao N, Rani G, Bakardjieva S and Subrt J 2010 Thick film titania on glass supports for vapour phase photocatalytic degradation of toluene , acetone , and ethanol *Chem. Eng. J.* **163** 219–29

[49] Chen W and Zhang J S 2008 UV-PCO device for indoor VOCs removal: investigation on multiple compounds effect *Build. Environ.* **43** 246–52

[50] Dong F, Wang Z, Li Y, Ho W and Lee S C 2014 Immobilization of polymeric g-C_3N_4 on structured ceramic foam for efficient visible light photocatalytic air purification with real indoor illumination *Environ. Sci. Technol.* **48** 10345–53

[51] Wang P, Wang J, Ming T, Wang X, Yu H, Yu J and Wang Y 2013 Dye-sensitization-induced visible-light reduction of graphene oxide for the enhanced TiO_2 photocatalytic performance *Environ. Sci. Technol.* **48** 10345–53

[52] Akhavan O 2010 Photocatalytic reduction of graphene oxides hybridized by ZnO nanoparticles in ethanol *Carbon* **49** 11–8

[53] Akhavan O and Ghaderi E 2009 Photocatalytic reduction of graphene oxide nanosheets on TiO_2 thin film for photoinactivation of bacteria in solar light irradiation *J. Phys. Chem.* C **113** 20214–20

[54] Williams G, Seger B and Kamat P V 2008 TiO_2-graphene nanocomposites. UV-assisted photocatalytic reduction of graphene oxide *ACS Nano* **2** 1487–91

[55] Imamura K, Tsukahara H, Hamamichi K, Seto N, Hashimoto K and Kominami H 2013 Simultaneous production of aromatic aldehydes and dihydrogen by photocatalytic dehydrogenation of liquid alcohols over metal-loaded titanium (IV) oxide under oxidant- and solvent-free conditions *Appl. Catal.* A **450** 28–33

[56] Su F, Mathew S C, Lipner G, Fu X, Antonietti M, Blechert S and Wang X 2010 'mpg-C_3N_4 -catalyzed selective oxidation of alcohols using O_2 and visible light *J. Am. Chem. Soc.* **132** 16299–301

[57] Özcan L, Yurdakal S, Augugliaro V, Loddo V, Palmas S, Palmisano G and Palmisano L 2013 Photoelectrocatalytic selective oxidation of 4-methoxybenzyl alcohol in water by TiO_2 supported on titanium anodes *Appl. Catal.* B **132–133** 535–42

[58] Tan L L, Ong W J, Chai S P and Mohamed A R 2017 Photocatalytic reduction of CO_2 with H_2O over graphene oxide-supported oxygen-rich TiO_2 hybrid photocatalyst under visible light irradiation: process and kinetic studies *Chem. Eng. J.* **308** 248–55

[59] Xiong Z, Lei Z, Kuang C C, Chen X, Gong B, Zhao Y, Zhang J, Zheng C and Wu J C S 2017 Selective photocatalytic reduction of CO_2 into CH_4 over Pt–Cu_2O TiO_2 nanocrystals: the interaction between Pt and Cu_2O cocatalysts *Appl. Catal.* B **202** 695–703

[60] Nikokavoura A and Trapalis C 2017 Alternative photocatalysts to TiO_2 for the photocatalytic reduction of CO_2 *Appl. Surf. Sci.* **391** 149–74

[61] Kou J, Lu C, Wang J, Chen Y, Xu Z and Varma R S 2017 Selectivity enhancement in heterogeneous photocatalytic transformations *Chem. Rev.* **117** 1445–515

[62] Mahmoudi M, Sant S, Wang B, Laurent S and Sen T 2011 Superparamagnetic iron oxide nanoparticles (SPIONs): development, surface modification and applications in chemotherapy *Adv. Drug Deliv. Rev.* **63** 24–46

[63] Shen Y F, Tang J, Nie Z H, Wang Y D, Ren Y and Zuo L 2009 Preparation and application of magnetic Fe_3O_4 nanoparticles for wastewater purification *Sep. Purif. Technol.* **68** 312–9

[64] Tju H, Taufik A and Saleh R 2016 Enhanced UV photocatalytic performance of magnetic Fe_3O_4/CuO/ZnO/NGP nanocomposites *J. Phys.: Conf. Ser.* **710** 1–6

[65] Taufik A and Saleh R 2016 Comparison of catalytic activities for photocatalytic and sonocatalytic degradation of organic dye in the presence of ternary Fe_3O_4/ZnO/CuO magnetic heteregenous nanocatalyst *AIP. Conf. Proc.* **1725** 1–6

[66] Weiss N O, Zhou H, Liao L, Liu Y, Jiang S, Huang Y and Duan X 2012 Graphene: an emerging electronic material *Adv. Mater.* **24** 5782–825

[67] Kochameshki M G, Marjani A, Mahmoudian M and Farhadi K 2017 Grafting of diallyldimethylammonium chloride on graphene oxide by RAFT polymerization for modification of nanocomposite polysulfone membranes using in water treatment *Chem. Eng. J.* **309** 206–21

[68] Mclaren A, Valdes-Solis T, Li G and Tsang S C 2009 Shape and size effects of ZnO nanocrystals on photocatalytic activity *J. Am. Chem. Soc.* **131** 12540–1

[69] Ge J, Lan M, Liu W, Jia Q, Guo L, Zhou B, Meng X, Niu G and Wang P 2016 Graphene quantum dots as efficient, metal-free, visible -light-active photocatalysts *Sci. China Mater.* **59** 12–9

[70] Liu B and Aydil E S 2009 Growth of oriented single-crystalline rutile TiO_2 nanorods on transparent conducting substrates for dye-sensitized solar cells *J. Am. Chem. Soc.* **131** 3985–90

[71] Basnet P, Larsen G K, Jadeja R P, Hung Y C and Zhao Y 2013 α-Fe_2O_3 nanocolumns and nanorods fabricated by electron beam evaporation for visible light photocatalytic and antimicrobial applications *ACS Appl. Mater. Interfaces* **5** 2085–95

[72] Shaban M, Ashraf A M and Abukhadra M R 2018 TiO_2 nanoribbons/carbon nanotubes composite with enhanced photocatalytic activity; fabrication, characterization, and application *Sci. Rep.* **8** 781

[73] Xiang Q, Yu J and Jaroniec M 2012 Graphene-based semiconductor photocatalysts *Chem. Soc. Rev.* **41** 782–96

[74] Suárez-Iglesias O, Collado S, Oulego P and Díaz M 2017 Graphene-family nanomaterials in wastewater treatment plants *Chem. Eng. J.* **313** 121–35

[75] Zhou Y, Li D, Yang L, Li C, Liu Y, Lu J and Wang Y 2017 Preparation of 3D urchin-like RGO/ZnO and its photocatalytic activity *J. Mater. Sci., Mater. Electron.* **28** 7935–42

[76] Luan V H, Tien H N and Hur S H 2015 Fabrication of 3D structured ZnO nanorod/reduced graphene oxide hydrogels and their use for photo-enhanced organic dye removal *J. Colloid Interface Sci.* **437** 181–6

[77] Chaudhuri R G and Paria S 2012 Core/shell nanoparticles: classes, properties, synthesis mechanisms, characterization, and applications *Chem. Rev.* **112** 2373–433

[78] Zhong C J and Maye M M 2001 Core–shell assembled nanoparticles as catalysts *Adv. Mater.* **13** 1507–11

[79] Wu Y, He T, Xu W and Li Y 2016 Preparation and photocatalytic activity of magnetically separable Fe_3O_4@ZnO nanospheres *J. Mater. Sci., Mater. Electron.* **27** 12155–9

[80] Gao S, Wang W, Ni Y, Lu C and Xu Z 2015 Facet-dependent photocatalytic mechanisms of anatase TiO_2: a new sight on the self-adjusted surface heterojunction *J. Alloys Compd.* **647** 981–8

[81] Han X, Kuang Q, Jin M, Xie Z and Zheng L 2009 Synthesis of titania nanosheets with a high percentage of exposed (001) facets and related photocatalytic properties *J. Am. Chem. Soc.* **131** 3152–3

[82] Hong Y, Jiang Y, Li C, Fan W, Yan X, Yan M and Shi W 2016 *In-situ* synthesis of direct solid-state Z-scheme V_2O_5/g–C_3N_4 heterojunctions with enhanced visible light efficiency in photocatalytic degradation of pollutants *Appl. Catal.* B **180** 663–73

[83] Fu J, Cao S and Yu J 2015 Dual Z-scheme charge transfer in TiO_2–Ag–Cu_2O composite for enhanced photocatalytic hydrogen generation *J. Mater.* **1** 124–33

[84] Bai X, Sun C, Liu D, Luo X, Li D, Wang J, Wang N, Chang X, Zong R and Zhu Y 2017 Photocatalytic degradation of deoxynivalenol using graphene/ZnO hybrids in aqueous suspension *Appl. Catal.* B **204** 11–20

[85] Rong X, Qiu F, Zhang C, Fu L, Wang Y and Yang D 2015 Preparation, characterization and photocatalytic application of TiO_2-graphene photocatalyst under visible light irradiation *Ceram. Int.* **41** 2502–11

[86] Park J, Jin T, Liu C, Li G and Yan M 2016 Three-dimensional graphene-TiO_2 nanocomposite photocatalyst synthesized by covalent attachment *ACS Omega* **1** 351–6

[87] Bai X, Wang L, Zong R, Lv Y, Sun Y and Zhu Y 2013 Performance enhancement of ZnO photocatalyst via synergic effect of surface oxygen defect and graphene hybridization *Langmuir* **29** 3097–105

[88] Costa dos Reis L, Vidal L and Canals A 2017 Graphene oxide/Fe_3O_4 as sorbent for magnetic solid-phase extraction coupled with liquid chromatography to determine 2,4,6-trinitrotoluene in water samples *Anal. Bioanal. Chem.* **409** 2665–74

[89] Sun Z, Guo J, Zhu S, Mao L, Ma J and Zhang D 2014 A high-performance Bi_2WO_6 –graphene photocatalyst for visible light-induced H_2 and O_2 generation *Nanoscale* **6** 2186–93

[90] Nanakkal A R and Alexander L K 2017 Graphene/$BiVO_4$/TiO_2 nanocomposite: tuning band gap energies for superior photocatalytic activity under visible light *J. Mater. Sci.* **52** 7997–8006

[91] Kuai L, Zhou Y, Tu W, Li P, Wang X Y, Xu Q, Li H, Xiao M and Tang L 2015 Rational construction of CdS/reduced graphene oxide/TiO_2 coreshell nanostructure as an all-solid-state Z-scheme system for CO_2 photoreduction into solar fuels *RSC Adv.* **5** 88409–13

[92] Zhang H, Lv X, Li Y, Wang Y and Li J 2009 P25 graphene composite as a high performance photocatalyst *ACS Nano* **4** 380–6

[93] Fu R and Zhu M 2016 Synthesis and characterization of the structure of Fe_3O_4 @ Graphene oxide nanocomposites *J. Mater. Sci.* **2** 4–7

[94] Ruales-Lonfat C, Barona J F, Sienkiewicz A, Bensimon M, Vélez-Colmenares J, Benítez N and Pulgarín C 2015 Iron oxides semiconductors are efficients for solar water disinfection: a comparison with photo-Fenton processes at neutral pH *Appl. Catal.* B **166–167** 497–508

[95] Effenberger F B, Couto R A, Kiyohara P K, Machado G, Masunaga S H, Jardim R F and Rossi L M 2017 Economically attractive route for the preparation of high quality magnetic nanoparticles by the thermal decomposition of iron(III) acetylacetonate *Nanotechnology* **28** 115603

[96] Liang Y J, Fan F, Ma M, Sun J, Chen J, Zhang Y and Gu N 2017 Size-dependent electromagnetic properties and the related simulations of Fe_3O_4 nanoparticles made by microwave-assisted thermal decomposition *Colloids Surf.* A **530** 191–9

[97] Li L, Qi G, Fukushima M, Wang B, Xu H and Wang Y 2017 Insight into the preparation of Fe_3O_4 nanoparticle pillared layered double hydroxides composite via thermal decomposition and reconstruction *Appl. Clay Sci.* **140** 88–95

[98] Unni M, Uhl A M, Savliwala S, Savitzky B H, Dhavalikar R, Garraud N, Arnold D P, Kourkoutis L F, Andrew J S and Rinaldi C 2017 Thermal decomposition synthesis of iron oxide nanoparticles with diminished magnetic dead layer by controlled addition of oxygen *ACS Nano* **11** 2284–303

[99] Saffari J, Mir N and Ghanbari D 2015 Sonochemical synthesis of Fe_3O_4/ZnO magnetic nanocomposites and their application in photo-catalytic degradation of various organic dyes *J. Mater. Sci., Mater. Electron.* **25** 9591–9

[100] Yu J, Yu X, Huang B, Zhang X and Dai Y 2009 Hydrothermal synthesis and visible-light photocatalytic activity of novel cage-like ferric oxide hollow spheres *Cryst. Growth Des.* **9** 2–8

[101] Yu X, Cheng G and Zheng S Y 2016 Synthesis of self-assembled multifunctional nanocomposite catalysts with highly stabilized reactivity and magnetic recyclability *Sci. Rep.* **6** 1–11

[102] Wang J, Yang J, Li X, Wang D, Wei B, Song H, Li X and Fu S 2016 Preparation and photocatalytic properties of magnetically reusable Fe_3O_4@ZnO core/shell nanoparticles *Physica* E **75** 66–71

[103] Shekofteh-Gohari M and Habibi-Yangjeh A 2017 Fe_3O_4/ZnO/$CoWO_4$ nanocomposites: novel magnetically separable visible-light-driven photocatalysts with enhanced activity in degradation of different dye pollutants *Ceram. Int.* **43** 3063–71

[104] Xia D and Lo I M C 2016 Synthesis of magnetically separable Bi_2O_4/Fe_3O_4hybrid nanocomposites with enhanced photocatalytic removal of ibuprofen under visible light irradiation *Water Res.* **100** 393–404

[105] Zhu Y, Xue J, Xu T, He G and Chen H 2017 Enhanced photocatalytic activity of magnetic core–shell Fe_3O_4@Bi_2O_3–RGO heterojunctions for quinolone antibiotics degradation under visible light *J. Mater. Sci., Mater. Electron.* **28** 8519–28

[106] Thangavel S, Thangavel S, Raghavan N, Krishnamoorthy K and Venugopal G 2016 Visible-light driven photocatalytic degradation of methylene-violet by rGO/Fe_3O_4/ZnO ternary nanohybrid structures *J. Alloys Compd.* **665** 107–12

[107] Lee K M, Lai C W, Ngai K S and Juan J C 2015 Recent developments of zinc oxide based photocatalyst in water treatment technology: a review *Water Res.* **88** 428–48

[108] Gu X, Li C, Yuan S, Ma M, Qiang Y and Zhu J 2016 ZnO based heterojunctions and their application in environmental photocatalysis *Nanotechnology* **27** 1–21

[109] Xu L, Hu Y L, Pelligra C, Chen C H, Jin L, Huang H, Sithambaram S, Aindow M, Joesten R and Suib S L 2009 ZnO with different morphologies synthesized by solvothermal methods for enhanced photocatalytic activity *Chem. Mater.* **21** 2875–85

[110] Hong J-I, Bae J, Wang Z L and Snyder R L 2009 Room-temperature, texture-controlled growth of ZnO thin films and their application for growing aligned ZnO nanowire arrays *Nanotechnology* **20** 85609

[111] Khalil A, Gondal M A and Dastageer M A 2011 Augmented photocatalytic activity of palladium incorporated ZnO nanoparticles in the disinfection of *Escherichia coli* microorganism from water *Appl. Catal.* A **402** 162–7

[112] Ren S, Zhao G, Wang Y, Wang B and Wang Q 2015 Enhanced photocatalytic performance of sandwiched ZnO@Ag@Cu_2O nanorod films: the distinct role of Ag NPs in the visible light and UV region *Nanotechnology* **26** 1–10

[113] Han C, Chen Z, Zhang N, Colmenares J C and Xu Y J 2015 Hierarchically CdS decorated 1D ZnO nanorods-2D graphene hybrids: low temperature synthesis and enhanced photocatalytic performance *Adv. Funct. Mater.* **25** 221–9

[114] Rokhsat E and Akhavan O 2016 Improving the photocatalytic activity of graphene oxide/ZnO nanorod films by UV irradiation *Appl. Surf. Sci.* **371** 592–5

[115] Lee J E, Khoa N T, Kim S W, Kim E J and Hahn S H 2015 Fabrication of Au/GO/ZnO composite nanostructures with excellent photocatalytic performance *Mater. Chem. Phys.* **164** 29–35

[116] Hashimoto K, Irie H and Fujishima A 2007 TiO_2 photocatalysis: a historical overview and future prospects *Japan. J. Appl. Phys* **17** 12–28

[117] Vereb G, Manczinger L, Bozso G, Sienkiewicz A, Forro L, Mogyorosi K, Hernadi K and Dombi A 2013 Comparison of the photocatalytic efficiencies of bare and doped rutile and anatase TiO_2 photocatalysts under visible light for phenol degradation and *E. coli* inactivation *Appl. Catal.* B **129** 566–74

[118] García-Fernández I, Fernández-Calderero I, Inmaculada Polo-López M and Fernández-Ibáñez P 2015 Disinfection of urban effluents using solar TiO_2 photocatalysis: a study of significance of dissolved oxygen, temperature, type of microorganism and water matrix *Catal. Today* **240** 30–8

[119] Fagan R, McCormack D E, Dionysiou D D and Pillai S C 2016 A review of solar and visible light active TiO_2 photocatalysis for treating bacteria, cyanotoxins and contaminants of emerging concern *Mater. Sci. Semicond. Process.* **42** 2–14

[120] Farghali A A, Zaki A H and Khedr M H 2016 Control of selectivity in heterogeneous photocatalysis by tuning TiO_2 morphology for water treatment applications *Nanomater. Nanotechnol.* **6** 1–6

[121] Yasmina M, Mourad K, Mohammed S H and Khaoula C 2014 Treatment heterogeneous photocatalysis; factors influencing the photocatalytic degradation by TiO_2 *Energy Proc.* **50** 559–66

[122] Han D Q, Hua Z H and Han Y S 2016 Hydrothermal synthesis and photoluminescence properties of Fe_3O_4/ZnO heterostructures *Mater. Res. Innov.* **20** 165–9

[123] Mills A, Davies R H and Worsley D 1993 Water purification by semiconductor photocatalysis *Chem. Soc. Rev.* **22** 417

[124] Welch K, Cai Y, Engqvist H and Strømme M 2010 Dental adhesives with bioactive and on-demand bactericidal properties *Dent. Mater.* **26** 491–9

[125] Mohamed H H and Mohamed S K 2018 Rutile TiO_2 nanorods/MWCNT composites for enhanced simultaneous photocatalytic oxidation of organic dyes and reduction of metal ions *Mater. Res. Express* **5** 1–9

[126] Guo X, Chen C, Song W, Wang X, Di W and Qin W 2014 CdS embedded TiO_2 hybrid nanospheres for visible light photocatalysis *J. Mol. Catal.* A **387** 1–6

[127] Zada I, Zhang W, Zheng W, Zhu Y, Zhang Z, Zhang J, Imtiaz M, Abbas W and Zhang D 2017 The highly efficient photocatalytic and light harvesting property of Ag–TiO_2 with negative nano-holes structure inspired from cicada wings *Sci. Rep.* **7** 1–9

[128] Momeni M M and Ghayeb Y 2015 Visible light activity of sulfur-doped TiO_2 nanostructure photoelectrodes prepared by single-step electrochemical anodizing process *J. Solid State Electrochem.* **19** 1359–66

[129] Yu B, Lau W M and Yang J 2013 Preparation and characterization of N–TiO_2 photocatalyst with high crystallinity and enhanced photocatalytic inactivation of bacteria *Nanotechnology* **24** 1–10

[130] Monteiro R A R, Miranda S M, Vilar V J P, Pastrana-Martínez L M, Tavares P B, Boaventura R A R, Faria J L, Pinto E and Silva A M T 2015 N-modified TiO_2 photocatalytic activity towards diphenhydramine

degradation and *Escherichia coli* inactivation in aqueous solutions *Appl. Catal.* B **162** 66–74
[131] Fisher M B, Keane D A, Fernández-Ibáñez P, Colreavy J, Hinder S J, McGuigan K G and Pillai S C 2013 Nitrogen and copper doped solar light active TiO_2 photocatalysts for water decontamination *Appl. Catal.* B **130–131** 8–13
[132] Xiang Q and Jaroniec M 2011 Nitrogen and sulfur co-doped TiO_2 nanosheets with exposed {001} facets: synthesis , characterization and visible-light photocatalytic activity *Phys. Chem. Chem. Phys.* **13** 4853–61
[133] Gong X, Wang H, Yang C, Li Q, Chen X and Hu J 2015 Photocatalytic degradation of high ammonia concentration wastewater by TiO_2 *Future Cities Environ.* **1** 1–12
[134] Rizzo L, Della Sala A, Fiorentino A and Li Puma G 2014 Disinfection of urban wastewater by solar driven and UV lamp—TiO_2 photocatalysis: effect on a multi drug resistant *Escherichia coli* strain *Water Res.* **53** 145–52
[135] Luo J, Wang S, Liu W, Tian C, Wu J, Zu X, Zhou W, Yuan X and Xiang X 2017 Influence of different aluminum salts on the photocatalytic properties of Al doped TiO_2 nanoparticles towards the degradation of AO7 dye *Sci. Rep.* **7** 8108
[136] Zhu Y, Murali S, Cai W, Li X, Suk J W, Potts J R and Ruoff R S 2010 Graphene and graphene oxide: synthesis, properties, and applications *Adv. Mater.* **22** 3906–24
[137] Zhang N and Xu Y J 2016 The endeavour to advance graphene-semiconductor composite-based photocatalysis *CrystEngComm* **18** 24–37
[138] Fernández-Ibáñez P *et al* 2015 Solar photocatalytic disinfection of water using titanium dioxide graphene composites *Chem. Eng. J.* **261** 36–44
[139] Lai C *et al* 2016 Synthesis of surface molecular imprinted TiO_2/graphene photocatalyst and its highly efficient photocatalytic degradation of target pollutant under visible light irradiation *Appl. Surf. Sci.* **390** 368–76
[140] Jiang G, Lin Z, Chen C, Zhu L, Chang Q, Wang N, Wei W and Tang H 2011 TiO_2 nanoparticles assembled on graphene oxide nanosheets with high photocatalytic activity for removal of pollutants *Carbon* **49** 2693–701
[141] Khalid N R, Ahmed E, Hong Z, Sana L and Ahmed M 2013 Enhanced photocatalytic activity of graphene-TiO_2 composite under visible light irradiation *Curr. Appl. Phys.* **13** 659–63
[142] Yang Y, Xu L, Wang H, Wang W and Zhang L 2016 TiO_2/graphene porous composite and its photocatalytic degradation of methylene blue *Mater. Des.* **108** 632–9
[143] Jo W K, Kumar S, Isaacs M A, Lee A F and Karthikeyan S 2017 Cobalt promoted TiO_2/GO for the photocatalytic degradation of oxytetracycline and Congo Red *Appl. Catal.* B **201** 159–68
[144] Wang W, Xiao K, Zhu L, Yin Y and Wang Z 2017 Graphene oxide supported titanium dioxide & ferroferric oxide hybrid, a magnetically separable photocatalyst with enhanced photocatalytic activity for tetracycline hydrochloride degradation *RSC Adv.* **7** 21287–97
[145] Yu H, Shi R, Zhao Y, Waterhouse G I N, Wu L Z, Tung C H and Zhang T 2016 Smart utilization of carbon dots in semiconductor photocatalysis *Adv. Mater.* **28** 9454–77
[146] Lee H U *et al* 2014 Highly photocatalytic performance of flexible 3-dimensional (3D) ZnO nanocomposite *Appl. Catal.* B **144** 83–9
[147] Sun X, Sheng L, Yang J, An K, Yu L and Zhao X 2017 Three-dimensional (3D) reduced graphene oxide (RGO)/zinc oxide (ZnO)/barium ferrite nanocomposites for electromagnetic absorption *J. Mater. Sci., Mater. Electron.* **28** 12900–8
[148] Wu F, Xia Y, Wang Y and Wang M 2014 Two-step reduction of self-assembed three-dimensional (3D) reduced graphene oxide (RGO)/zinc oxide (ZnO) nanocomposites for electromagnetic absorption *J. Mater. Chem.* A **2** 20307–15
[149] Chiou Y-D and Hsu Y-J 2011 Room-temperature synthesis of single-crystalline Se nanorods with remarkable photocatalytic properties *Appl. Catal.* B **105** 211–9
[150] Xia D, Shen Z, Huang G, Wang W, Yu J C and Wong P K 2015 Red phosphorus: an earth-abundant elemental photocatalyst for 'green' bacterial inactivation under visible light *Environ. Sci. Technol.* **49** 6264–73
[151] Chan D K L, Yu J C, Li Y and Hu Z 2017 A metal-free composite photocatalyst of graphene quantum dots deposited on red phosphorus *J. Environ. Sci.* **60** 91–7
[152] Yang X, Ye X and Liu C 2018 Monolayer CS as a metal-free photocatalyst with high carrier mobility and tunable band structure: a first-principles study *J. Phys.: Condens. Matter* **30** 1–12
[153] Liu J, Wen S, Hou Y, Zuo F, Beran G J O and Feng P 2013 Boron carbides as efficient, metal-free, visible-light-responsive photocatalysts *Angew. Chem., Int. Ed.* **52** 3241–5
[154] Xin G and Meng Y 2013 Pyrolysis synthesized g-C_3N_4 for photocatalytic degradation of methylene blue *J. Chem.* **2013** 1–5
[155] Xu H Y, Wu L C, Zhao H, Jin L G and Qi S Y 2015 Synergic effect between adsorption and photocatalysis of metal-free g-C_3N_4 derived from different precursors *PLoS One* **10** 1–20
[156] Kang Z, Tsang C H A, Wong N-B, Zhang Z and Lee S-T 2007 Silicon quantum dots: a general photocatalyst for reduction, decomposition, and selective oxidation reactions *J. Am. Chem. Soc.* **129** 12090–1
[157] Stolbov S and Zuluaga S 2013 Sulfur doping effects on the electronic and geometric structures of graphitic carbon nitride photocatalyst: insights from first principles *J. Phys.: Condens. Matter* **25** 1–7
[158] Cui Y, Huang J, Fu X and Wang X 2012 Metal-free photocatalytic degradation of 4-chlorophenol in water by mesoporous carbon nitride semiconductors *Catal. Sci. Technol.* **2** 1396
[159] Zhang Q, Wang H, Li Z, Geng C and Leng J 2017 Metal-free photocatalyst with visible-light-driven post-illumination catalytic memory *ACS Appl. Mater. Interfaces* **9** 21738–46
[160] Purohit B, Kumawat S and Dixit A 2018 Enhancement in photocatalytic response of inorganic–organic enhancement in photocatalytic response of inorganic–organic $BiVO_4/C_3N_4$ composite system *Mater. Res. Express* **5** 0–7
[161] Zhang H, Zhao L, Geng F, Guo L H, Wan B and Yang Y 2016 Carbon dots decorated graphitic carbon nitride as an efficient metal-free photocatalyst for phenol degradation *Appl. Catal.* B **180** 656–62
[162] Zhu Z, Lu Z, Wang D, Tang X, Yan Y, Shi W, Wang Y, Gao N, Yao X and Dong H 2016 Construction of high-dispersed Ag/Fe_3O_4/g-C_3N_4photocatalyst by selective photo-deposition and improved photocatalytic activity *Appl. Catal.* B **182** 115–22
[163] Mousavi M and Habibi-Yangjeh A 2016 Magnetically separable ternary g-C_3N_4/Fe_3O_4/BiOI nanocomposites: novel visible-light-driven photocatalysts based on graphitic carbon nitride *J. Colloid Interface Sci.* **465** 83–92
[164] Mahmood J *et al* 2015 Nitrogenated holey two-dimensional structures *Nat. Commun.* **6** 1–7
[165] Yu S, Rao Y C and Duan X M 2017 Modulating the properties of monolayer C_2N: a promising metal-free photocatalyst for water splitting *Chin. Phys.* B **26** 6–11
[166] Yin X-L, Liu J, Jiang W-J, Zhang X, Hu J-S and Wan L-J 2015 Urchin-like Au@CdS/WO_3 micro/nano heterostructure as a visible-light driven photocatalyst for efficient hydrogen generation *Chem. Commun.* **51** 13842–5
[167] Balayeva N O, Fleisch M and Bahnemann D W 2017 Surface-grafted WO_3/TiO_2 photocatalysts: enhanced visible-light

activity towards indoor air purification *Catal. Today* (https://doi.org/10.1016/j.cattod.2017.12.008)
[168] Zhu W, Sun F, Goei R and Zhou Y 2017 Facile fabrication of RGO-WO_3 composites for effective visible light photocatalytic degradation of sulfamethoxazole *Appl. Catal.* B **207** 93–102
[169] Aguilera-Ruiz E, García-Pérez U M, De La Garza-Galván M, Zambrano-Robledo P, Bermúdez-Reyes B and Peral J 2015 Efficiency of $Cu_2O/BiVO_4$ particles prepared with a new soft procedure on the degradation of dyes under visible-light irradiation *Appl. Surf. Sci.* **328** 361–7
[170] Zou W, Zhang L, Liu L, Wang X, Sun J, Wu S, Deng Y, Tang C, Gao F and Dong L 2016 Engineering the Cu_2O-reduced graphene oxide interface to enhance photocatalytic degradation of organic pollutants under visible light *Appl. Catal.* B **181** 495–503
[171] Miller E B, Zahran E M, Knecht M R and Bachas L G 2017 Metal oxide semiconductor nanomaterial for reductive debromination: visible light degradation of polybrominated diphenyl ethers by Cu_2O@Pd nanostructures *Appl. Catal.* B **213** 147–54
[172] Ali F, Khan S B, Kama T, Alamry K A and Asiri A M 2018 Chitosan-titanium oxide fibers supported zero-valent nanoparticles: highly efficient and easily retrievable catalyst for the removal of organic pollutants *Sci. Rep.* **8** 1–18
[173] Saravanan R, Sacari E, Gracia F, Khan M M, Mosquera E and Gupta V K 2016 Conducting PANI stimulated ZnO system for visible light photocatalytic degradation of coloured dyes *J. Mol. Liq.* **221** 1029–33
[174] Koushkbaghi S, Zakialamdari A, Pishnamazi M, Ramandi H F, Aliabadi M and Irani M 2018 Aminated-Fe_3O_4 nanoparticles filled chitosan/PVA/PES dual layers nanofibrous membrane for the removal of Cr(VI) and Pb(II) ions from aqueous solutions in adsorption and membrane processes *Chem. Eng. J.* **337** 169–82
[175] Wang C, Ao Y, Wang P, Zhang S, Qian J and Hou J 2010 A simple method for large-scale preparation of ZnS nanoribbon film and its photocatalytic activity for dye degradation *Appl. Surf. Sci.* **256** 4125–8
[176] Ye Z, Kong L, Chen F, Chen Z, Lin Y and Liu C 2018 A comparative study of photocatalytic activity of ZnS photocatalyst for degradation of various dyes *Optik* **164** 345–54
[177] Reddy D A, Ma R, Yong M and Kyu T 2015 Applied surface science reduced graphene oxide wrapped ZnS—Ag_2S ternary composites synthesized via hydrothermal method: applications in photocatalyst degradation of organic pollutants *Appl. Surf. Sci.* **324** 725–35
[178] Li Q, Li X, Wageh S, Al-ghamdi A A and Yu J 2015 CdS/graphene nanocomposite photocatalysts *Adv. Energy Mater.* **5** 1–28
[179] Maria Magdalane C, Kaviyarasu K, Judith Vijaya J, Jayakumar C, Maaza M and Jeyaraj B 2017 Photocatalytic degradation effect of malachite green and catalytic hydrogenation by UV-illuminated CeO_2/CdO multilayered nanoplatelet arrays: investigation of antifungal and antimicrobial activities *J. Photochem. Photobiol.* B **169** 110–23
[180] Liu L, Ding L, Liu Y, An W, Lin S, Liang Y and Cui W 2017 A stable Ag_3PO_4@PANI core@shell hybrid: enrichment photocatalytic degradation with π–π conjugation *Appl. Catal.* B **201** 92–104
[181] Kumar A, Sharma G, Naushad M and Thakur S 2015 SPION/β-cyclodextrin core–shell nanostructures for oil spill remediation and organic pollutant removal from waste water *Chem. Eng. J.* **280** 175–87
[182] Korina E, Stoilova O, Manolova N and Rashkov I 2018 Polymer fibers with magnetic core decorated with titanium dioxide prospective for photocatalytic water treatment *J. Environ. Chem. Eng.* **6** 2075–84
[183] Mohamed A, Yousef S, Ali Abdelnaby M, Osman T A, Hamawandi B, Toprak M S, Muhammed M and Uheida A 2017 Photocatalytic degradation of organic dyes and enhanced mechanical properties of PAN/CNTs composite nanofibers *Sep. Purif. Technol.* **182** 219–23
[184] Jo W K and Selvam N C S 2017 Z-scheme CdS/g-C_3N_4composites with RGO as an electron mediator for efficient photocatalytic H_2 production and pollutant degradation *Chem. Eng. J.* **317** 913–24
[185] Fang Z, Liu Y, Fan Y, Ni Y, Wei X, Tang K, Shen J and Chen Y 2011 Epitaxial growth of CdS nanoparticle on Bi_2S_3 nanowire and photocatalytic application of the heterostructure *J. Phys. Chem.* C **115** 13968–76
[186] Fkiri A, Mezni A and Smiri L S 2018 Facile synthesis of Cu doped Au–ZnS photocatalyst *J. Inorg. Organomet. Polym. Mater.* **28** 27–34
[187] Babu S G, Vijayan A S, Neppolian B and Ashokkumar M 2015 SnS_2/rGO: an efficient photocatalyst for the complete degradation of organic contaminants *Mater. Focus* **4** 272–6
[188] Choi J, Reddy D A and Kim T K 2015 Enhanced photocatalytic activity and anti-photocorrosion of AgI nanostructures by coupling with graphene-analogue boron nitride nanosheets *Ceram. Int.* **41** 1–11
[189] Pirila M, Saouabe M, Ojala S, Rathnayake B, Drault F, Valtanen A, Huuhtanen M, Brahme R and Keiski R L 2015 Photocatalytic degradation of organic pollutants in wastewater *Top Catal.* **68** 1085–99
[190] Ibhadon A O, Fitzpatrick P, Sciences M, Road C, Innovation C and Park C T 2013 Heterogeneous photocatalysis: recent advances and applications *Catalysts* **3** 1–29
[191] Rezaei M, Rashidi F, Royaee S J and Jafarikojous M 2014 Performance evaluation of a continuous flow photocatalytic reactor for wastewater treatment *Environ. Sci. Pollut. Res.* **21** 12505–17
[192] Abramovic B F, Banic N D and Krstic J B 2013 Degradation of thiacloprid by ZnO in a laminar falling film slurry photocatalytic reactor *Ind. Eng. Chem. Res.* **52** 5040–7
[193] Molinari R, Lavorato C and Argurio P 2017 Recent progress of photocatalytic membrane reactors in water treatment and in synthesis of organic compounds. A review *Catal. Today* **281** 144–64
[194] Molinari R, Mungari M, Drioli E, Di Paola A and Loddo V 2000 Study on a photocatalytic membrane reactor for water purification *Catal. Today* **55** 71–8
[195] Mukherjee P S and Ray A K 1999 Major challenges in the design of a large-scale photocatalytic reactor for water treatment *Chem. Eng. Technol.* **22** 253–60
[196] Fernandez A, Lassaletta G, Jimenez V M, Justo A, Gonzolez-Elipe A R, Herrmann J M, Tahiri H and Ait-Ichou Y 1995 Preparation and characterization of TiO_2 photocatalysts supported on various rigid supports (glass, quartz and stainless steel). Comparative studies of photocatalytic activity in water purification *Appl. Catal.* B **7** 49–63
[197] Delnavaz M, Ayati B, Ganjidoust H and Sanjabi S 2015 Application of concrete surfaces as novel substrate for immobilization of TiO_2 nano powder in photocatalytic treatment of phenolic water *J. Environ. Heal. Sci. Eng.* **13** 1–10
[198] Ao C H, Lee S C and Yu J C 2003 Photocatalyst TiO_2 supported on glass fiber for indoor air purification: effect of NO on the photodegradation of CO and NO_2 *J. Photochem. Photobiol.* A **156** 171–7
[199] Calia A, Lettieri M, Masieri M, Pal S, Licciulli A and Arima V 2017 Limestones coated with photocatalytic TiO_2

to enhance building surface with self-cleaning and depolluting abilities *J. Clean. Prod.* **165** 1036–47
[200] Zhao J, Wang J, Fan L, Pakdel E, Huang S and Wang X 2016 Immobilization of titanium dioxide on PAN fiber as a recyclable photocatalyst via co-dispersion solvent dip coating *Text. Res. J.* **87** 570–81
[201] Machida M, Norimoto K and Yamamoto M 2017 Control of the oxidizing and hydrophilicizing properties of photocatalytic TiO_2 thin films coated on a polyethylene-terephthalate substrate *J. Ceram. Soc. Japan* **125** 168–74
[202] Yadav M, Rhee K Y, Park S J and Hui D 2014 Mechanical properties of Fe_3O_4/GO/chitosan composites *Composites* B **66** 89–96
[203] Gad-Allah T A, Kato S, Satokawa S and Kojima T 2009 Treatment of synthetic dyes wastewater utilizing a magnetically separable photocatalyst (TiO_2/SiO_2/Fe_3O_4): parametric and kinetic studies *Desalination* **244** 1–11
[204] Andreozzi R, Caprio V, Insola A and Marotta R 1999 Advanced oxidation processes (AOP) for water purification and recovery *Catal. Today* **53** 51–9
[205] Houas A, Lachheb H, Ksibi M, Elaloui E, Guillard C and Herrmann J 2001 Photocatalytic degradation pathway of methylene blue in water *Appl. Catal.* B **31** 145–57
[206] Reza K M, Kurny A and Gulshan F 2017 Parameters affecting the photocatalytic degradation of dyes using TiO_2: a review *Appl. Water Sci.* **7** 1569–78
[207] Dong S, Feng J, Fan M, Pi Y, Hu L, Liu M, Sun J and Sun J 2015 Recent developments in heterogeneous photocatalytic water treatment using visible-light-responsive photocatalysts: a review *RSC Adv.* **5** 14610–30
[208] Zhang Y, Zhang N, Tang Z R and Xu Y J 2012 Graphene transforms wide band gap ZnS to a visible light photocatalyst. the new role of graphene as a macromolecular photosensitizer *ACS Nano* **6** 9777–89
[209] Wang W, Serp P, Kalck P and Faria J L 2005 Visible light photodegradation of phenol on MWNT-TiO_2 composite catalysts prepared by a modified sol–gel method *J. Mol. Catal.* A **235** 194–9
[210] Molinari R, Palmisano L, Drioli E and Schiavello M 2002 Studies on various reactor configurations for coupling photocatalysis and membrane processes in water purification *J. Membr. Sci.* **206** 399–415
[211] Kertèsz S and Jiránková H 2014 Submerged hollow fiber micro filtration as a part of hybrid photocatalytic process for dye wastewater treatment *Desalination* **343** 106–12
[212] Gebregiorgis T, van Hullebusch E D and Hagos K 2018 Decolourization of real textile wastewater by the combination of photocatalytic and biological oxidation processes *Advances in Science, Technology & Innovation* (*IEREK Interdisciplinary Series for Sustainable Development*) (Cham: Springer) pp 115–7
[213] Ying Y, Ying W, Li Q, Meng D, Ren G, Yan R and Peng X 2017 Recent advances of nanomaterial-based membrane for water purification *Appl. Mater. Today* **7** 144–58
[214] Liu G, Han K, Ye H, Zhu C, Gao Y, Liu Y and Zhou Y 2017 Graphene oxide/triethanolamine modified titanate nanowires as photocatalytic membrane for water treatment *Chem. Eng. J.* **320** 74–80
[215] Zhang J, Xue Q, Pan X, Jin Y, Lu W, Ding D and Guo Q 2017 Graphene oxide/polyacrylonitrile fiber hierarchical-structured membrane for ultra-fast microfiltration of oil-water emulsion *Chem. Eng. J.* **307** 643–9
[216] Luo M L, Zhao J Q, Tang W and Pu C S 2005 Hydrophilic modification of poly(ether sulfone) ultrafiltration membrane surface by self-assembly of TiO_2 nanoparticles *Appl. Surf. Sci.* **249** 76–84
[217] Bae T H, Kim I C and Tak T M 2006 Preparation and characterization of fouling-resistant TiO_2 self-assembled nanocomposite membranes *J. Membr. Sci.* **275** 1–5
[218] Matthews R W 1987 Solar-electric water purification using photocatalytic oxidation with TiO_2 as a stationary phase *Sol. Energy* **38** 405–13
[219] Muñoz I, Rieradevall J, Torrades F, Peral J and Domènech X 2005 Environmental assessment of different solar driven advanced oxidation processes *Sol. Energy* **79** 369–75
[220] Muñoz I, Peral J, Antonio Ayllón J, Malato S, Passarinho P and Domènech X 2006 Life cycle assessment of a coupled solar photocatalytic-biological process for wastewater treatment *Water Res.* **40** 3533–40
[221] Yin R, Ling L, Xiang Y, Yang Y, Bokare A D and Shang C 2018 Enhanced photocatalytic reduction of chromium (VI) by Cu-doped TiO_2 under UV-A irradiation *Sep. Purif. Technol.* **190** 53–9
[222] Iervolino G, Vaiano V, Sannino D, Rizzo L, Galluzzi A, Polichetti M, Pepe G and Campiglia P 2018 Hydrogen production from glucose degradation in water and wastewater treated by Ru-$LaFeO_3$/Fe_2O_3 magnetic particles photocatalysis and heterogeneous photo-Fenton *Int. J. Hydrog. Energy* **43** 2184–96
[223] Booshehri A Y, Polo-Lopez M I, Castro-Alférez M, He P, Xu R, Rong W, Malato S and Fernández-Ibáñez P 2017 Assessment of solar photocatalysis using Ag/$BiVO_4$ at pilot solar compound parabolic collector for inactivation of pathogens in well water and secondary effluents *Catal. Today* **281** 124–34
[224] Ye Y, Feng Y, Bruning H, Yntema D and Rijnaarts H H M 2018 Photocatalytic degradation of metoprolol by TiO_2 nanotube arrays and UV-LED: effects of catalyst properties, operational parameters, commonly present water constituents, and photo-induced reactive species *Appl. Catal.* B **220** 171–81
[225] Deng Y, Tang L, Feng C, Zeng G, Wang J, Zhou Y, Liu Y, Peng B and Feng H 2018 Construction of plasmonic Ag modified phosphorous-doped ultrathin g-C_3N_4 nanosheets/$BiVO_4$ photocatalyst with enhanced visible-near-infrared response ability for ciprofloxacin degradation *J. Hazard. Mater.* **344** 758–69